nature communications

Article

https://doi.org/10.1038/s41467-024-52224-6

Maf expression in B cells restricts reactive plasmablast and germinal center B cell expansion

Received: 18 September 2023

Accepted: 29 August 2024

Published online: 12 September 2024

Check for updates

Sophie Hillion[1,2] ✉, Anjelica Miranda[2], Christelle Le Dantec[3], Marina Boudigou[3], Laëtitia Le Pottier[3], Divi Cornec[1], Raul M. Torres[2] & Roberta Pelanda[2]

Precise regulation of B cell differentiation is essential for an effective adaptive immune response. Here, we show that B cell development in mice with B cell-specific Maf deletion is unaffected, but marginal zone B cells, germinal centre B cells, and plasmablasts are significantly more frequent in the spleen of naive Maf-deficient mice compared to wild type controls. In the context of a T cell-dependent immunization, Maf deletion causes increased proliferation of germinal centre B cells and extrafollicular plasmablasts. This is accompanied by higher production of antigen-specific IgG1 antibodies with minimal modification of early memory B cells, but a reduction in plasma cell numbers. Single-cell RNA sequencing shows upregulation of genes associated with DNA replication and cell cycle progression, confirming the role of Maf in cell proliferation. Subsequent pathway analysis reveals that Maf influences cellular metabolism, transporter activity, and mitochondrial proteins, which have been implicated in controlling the germinal centre reaction. In summary, our findings demonstrate that Maf acts intrinsically in B cells as a negative regulator of late B cell differentiation, plasmablast proliferation and germinal centre B cell formation.

The transcription factor (TF) c-MAF (Maf), a member of the AP-1 superfamily and, more specifically, of the large Maf protein family[1], is a basic region-leucine zipper TF with a role in developmental processes[2]. In hematopoietic cells, Maf was initially identified as a Th2 restricted TF[3], but since then has emerged as a broad molecular regulator in many cell subsets including T cells[4], macrophages[5] and innate lymphoid cells[6]. Maf was described as a key factor regulating IL-10 production in T cells in different pathophysiological settings[7], but also as a master regulator of T follicular helper (Tfh) function[8,9], Th17 differentiation[10], and IL-27-induced regulatory T cells[11]. The role of Maf in B cells has been less clear. Mice harboring a deletion of Maf in all cells display slightly reduced IgG response to vaccination[3], while mice overexpressing Maf in B cells develop B cell lymphomas, plasma cell (PC) expansion, and monoclonal gammopathy[12]. Interestingly, genetic translocations with Maf overexpression are associated with multiple myeloma in humans[13]. Moreover, we and others recently proposed that Maf is associated with regulatory plasmablast (PB) cells and PB differentiation[14,15]. Overall, these data suggest a role of Maf in PB/PC differentiation, survival and/or proliferation. However, a large gap in knowledge remains regarding the intrinsic function of Maf in B cells.

To resolve the role Maf plays in B cells, we develop and investigate mice with a *Maf* deletion restricted to B lymphocytes. We report that Maf functions in a B cell-intrinsic way to control marginal zone B cell

[1]LBAI, UMR1227, Univ Brest, Inserm, and CHU de Brest, Brest, France. [2]Department of Immunology and Microbiology, University of Colorado School of Medicine, Anschutz Medical Campus, Aurora, CO 80045, USA. [3]LBAI, UMR1227, Univ Brest, Inserm, Brest, France. ✉e-mail: sophie.hillion@univ-brest.fr

development, B cell proliferation, and B cell responses to a T cell dependent (TD) antigen, likely regulating metabolic activities.

Results

Maf deletion increases numbers of marginal zone B cells, germinal center B cells and plasmablasts in naive mice

To identify the role of Maf in B-cell physiology, we crossed a Maf-floxed mouse model[16] with the CD19-cre strain[17] to generate a mouse lacking Maf expression specifically in the B cell lineage ($Maf^{flox/flox}$;CD19-cre, hereafter referred to as $Maf^{\Delta B}$). To confirm loss of Maf expression in B cells by flow cytometry, we first tested a previously validated commercial anti-Maf antibody with wild-type cells[18]. The staining intensity of Maf was above the isotype control in B cells and was higher in regulatory T cells and macrophages, displaying the highest signal in Tfh cells (Supplementary Fig. 1a) in accordance with the literature[9]. Nevertheless, there was no difference in the staining intensity of B cells from wild-type and $Maf^{\Delta B}$ mice (Supplementary Fig. 1a), indicating the detection threshold of this Ab might be too low. Unfortunately, other commercial Maf Abs displayed high non-specific staining, likely due to the high homology between all Maf family members. To demonstrate loss of the *Maf* allele by an alternate approach, we validated *Maf* gene deletion at the DNA level using primers that simultaneously amplified DNA fragments corresponding to the wild type, the floxed and the deleted *Maf* alleles. This PCR detected a strong Δ*Maf* band and a weak *Maf-flox* band in spleen B cells from homozygous $Maf^{\Delta B}$ mice (*Cre/+ fl/fl*), while both bands were equally amplified in B cells from heterozygous $Maf^{\Delta B}$ mice (*Cre/+ fl/+*) (Supplementary Fig. 1c). In contrast, this PCR amplified only the *Maf-flox* band in tail DNA from $Maf^{\Delta B}$ mice and the *Maf* WT band in cells from $CD19^{Cre}$ heterozygote control mice (*Cre/+*). Efficient deletion of the *Maf* gene in spleen B cells from $Maf^{\Delta B}$ mice was further confirmed at the RNA level by quantitative RT-PCR on cDNA (Supplementary Fig. 1d). To establish deletion efficiency, we crossed $Maf^{\Delta B}$ mice with R26-stop-EYFP mutant mice to generate mice in which the activity of Cre recombinase leads to the expression of EYFP. YFP was expressed in more than 95% of total B cells, follicular B cells, and marginal zone B cells in naïve $Maf^{\Delta B}$ R26-stop-$EYFP^{+/-}$ mice and in >95% of $B220^+$ $CD19^+Fas^+PNA^+$ cells (Germinal center, GC) and PBs cells in immunized mice (Supplementary Fig. 1e, f). Collectively, these results confirm the efficient deletion of Maf across different B-cell populations and that MAF-deleted B cells were not counter-selected through B cell development and differentiation.

We first investigated whether Maf deficiency alters B-cell maturation in the bone marrow (BM) by assessing the different B cell subsets (percentage and cell number) using staining based on the Hardy classification system[19]. There were no significant differences in total $B220^+$ cell numbers (Fig. 1a) or in the distribution and cell numbers of pro-B cells ($B220^+CD43^+$, including subsets fractions A-C') and pre-B cell fraction D ($B220^+CD43^-IgM^-$) in the absence or presence of Maf (Fig. 1b, c). There were also no differences in the frequency and number of immature B cells fraction E ($B220^+CD43^-IgM^+IgD^-$) and of mature recirculating B cells fraction F ($B220^+CD43^-IgM^{low}IgD^+$) (Fig. 1c), suggesting that Maf does not regulate B cell development in the bone marrow.

We then evaluated the impact of Maf-deletion in spleen B cells. Overall B-cell number was unchanged, with normal proportions of transitional ($CD93^{high}CD24^{high}$) and follicular ($CD21^+CD23^+$) B cells (Fig. 1d and Supplementary Fig. 2a). However, there was a two-fold increase of marginal zone B cells ($CD21^{high}CD1d^+$) in the $Maf^{\Delta B}$ mice in percentage and absolute number (Supplementary Fig. 1g). In addition, naïve $Maf^{\Delta B}$ mice revealed a significantly higher proportion and number of spontaneous GC B cells ($GL7^+Fas^+$) (Fig. 1e). Increased GC B cells correlated with a significant increase of Tfh cells ($CD4^+CXCR5^+PD1^+$) and $CD4^+Foxp3^+$ regulatory T cells (Fig. 1f, Supplementary Fig. 2b, c). The absence of Maf in B cells did not affect the distribution of other immune cells (Supplementary Fig. 2d, e). Naive $Maf^{\Delta B}$ mice displayed a two-fold increase of the $TACI^+CD138^+$ plasmablast (PB) population in the spleen (Fig. 1g), although there was no significant difference in the $Blimp1^+TACI^+$ PB and plasma cell (PC) compartment in the BM (Fig. 1h). Finally, Ig levels in serum in naive control and $Maf^{\Delta B}$ mice was determined by ELISA. The serum concentration of IgM was increased whereas that of IgG1 was slightly decreased (Supplementary Fig. 2f, g). Serum amounts of IgG2a and IgG2b (Supplementary Fig. 2h, i) were comparable in $Maf^{\Delta B}$ and control mice. Overall, these data show that Maf deletion does not alter B cell development or the generation of naïve B cells while it increases numbers of marginal zone B cells, germinal center B cells and PBs, which correlated with an increase of basal IgM production.

Deletion of Maf increases PB generation in vitro

To investigate the role of Maf in the generation of PBs, spleen B cells from $Maf^{\Delta B}$ and $CD19^{Cre/+}$ control mice were stimulated in vitro with either LPS[20] or anti-CD40 antibodies with IL-4 and IL-5[21] for 3 days. Cells were then analyzed for the expression of CD138, TACI and intracellular Blimp-1 to visualize activated B cells ($Blimp1^-CD138^-$), pre-PB cells ($Blimp1^+CD138^-$), and PBs ($Blimp1^+CD138^+$ or $TACI^+CD138^+$) (Fig. 2a, b). $Maf^{\Delta B}$ B cells displayed significantly increased viability following LPS stimulation (Supplementary Fig. 3a). Both stimulations resulted in a significantly higher frequency of PBs in cultures of $Maf^{\Delta B}$ B cells relative to control (Fig. 2a, b), without any significant modification of Blimp1 and CD138 mean fluorescence intensity. We then measured the effect of Maf deletion on the expression of the early (CD69) and late (CD86) activation markers. The deletion of Maf significantly increased the frequency of $CD69^+$ cells following anti-CD40, IL-4 and IL-5 stimulation, but did not change the frequency or level of CD86 expression (Fig. 2c). This suggests that Maf negatively regulates PB differentiation without affecting overall B-cell activation or Blimp1 and CD138 regulation.

Maf restrains the GC reaction and extra-follicular PB generation during T cell-dependent B cell responses

To investigate whether Maf regulates T cell-dependent B cell responses, we immunized $Maf^{\Delta B}$ and control mice with the hapten 4-hydroxy-3-nitrophenylacetyl (NP) conjugated to chicken gamma globulin (CGG)[22–25]. B cells responding to NP-CGG in BL/6 mice can be tracked by their ability to bind NP and/or their expression of lambda light chains. At day 7 post-immunization, there was increased proportion and number of PNA^+Fas^+ GC B cells and $CD138^+$ PBs in $Maf^{\Delta B}$ mice compared to $CD19^{Cre/+}$ controls (Fig. 3a, b). This difference persisted through day 10 post immunization and resolved by day 28 (Supplementary Fig. 3b). Among NP-binding B cells (Supplementary Fig. 3c), those from $Maf^{\Delta B}$ mice exhibited a higher proportion of extra-follicular (EF) PBs ($B220^{low}$ $CXCR5^{low}$ [26]), but a normal frequency of Fas^+PNA^+ GC cells (Fig. 3c, d). Among the NP-specific PB and GC B cell subsets there was a marked expansion of IgG1 switched cells in $Maf^{\Delta B}$ mice relative to controls (Fig. 3e, f). The increased proportion of NP IgG1 EF-PBs and of GC B cells in $Maf^{\Delta B}$ mice correlated with an increased concentration of NP-specific IgG1Abs (Fig. 3g) and, to a lesser extent, of NP-specific IgM and IgG2b Abs in sera (Fig. 3h, i).

We next evaluated TI-1 and TI-2 T cell-independent B cell responses. Maf deletion led to an expansion of PBs and total IgM production after TI-1 (LPS) challenge (Supplementary Fig. 3d), while there were no significant changes in NP-specific IgM or IgG2c production after NP-Ficoll (TI-2) immunization, even in the presence of poly:IC[27] (Supplementary Fig. 3e). These data suggest that Maf restrains extra-follicular PB cell generation and B-cell expansion within the GC after T-cell-dependent immunization.

Maf is involved in controlling B cells proliferation after initial activation

The observed expansion of EF-PBs following NP-CGG or LPS immunizations suggested an inhibitory function of Maf early upon B cell

https://doi.org/10.1038/s41467-024-52224-6

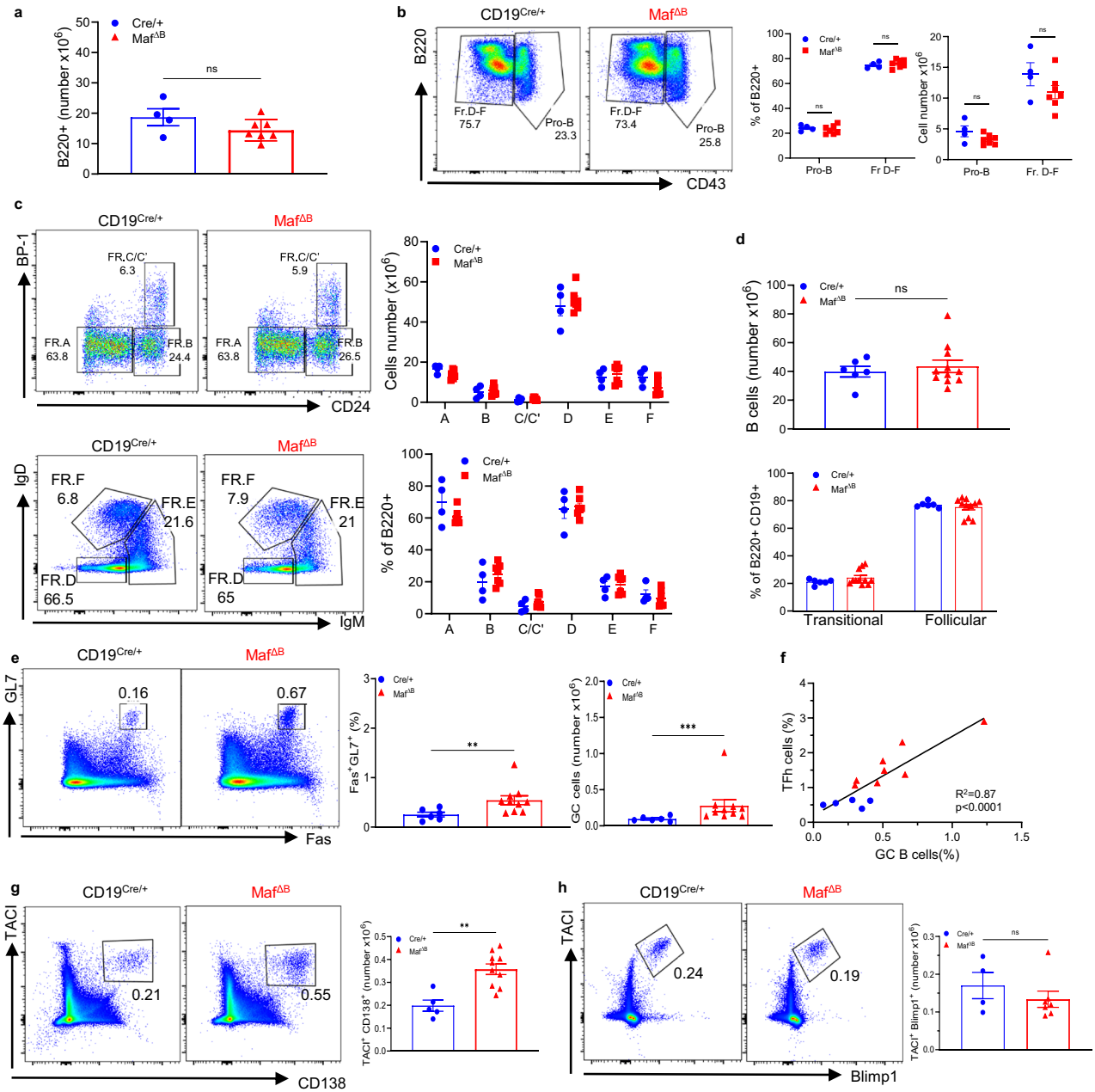

Fig. 1 | Mice with Maf deficiency in B cells exhibit more MZ B cells, spontaneous GC B cells and PB cell numbers in the spleen. Analysis of B cells from CD19$^{Cre/+}$ (Cre$^+$) and Maf$^{\Delta B}$ naïve mice in bone marrow (**a**–**c**, **h**, Cre$^+$: $N = 4$; Maf$^{\Delta B}$: $N = 7$) and in spleen (**d**–**g**; Cre$^+$: $N = 5$-6; Maf$^{\Delta B}$: $N = 10$-11). **a** Bar graphs showing total B220$^+$ cell counts. **b** Pseudocolor plots and bar graphs illustrating pro-B cells and pre-B to mature recirculating B cells (Fr. D-F, as described in ref. 19)in percentages and total cell numbers **c** Pseudocolor plots illustrating the Hardy's B cell fractions[19] and bar graphs showing percentages and total cell numbers of the different cell fractions. **d** Bar graphs showing total (CD19$^+$B220$^+$) B cell numbers and percentages of Transitional (CD24^{high}CD93^{high}) and follicular (CD21$^+$CD23$^+$) B cells gated on CD19$^+$B220$^+$ B cells. **e** Pseudocolor plots gating germinal center (GC) B cells gated on B220$^+$CD19$^+$ B cells and bar graphs showing percentages ($p = 0.008$) and number ($p = 0.0017$) of total GC B cells. **f** Plot showing total number of GC B cells and number of follicular helper T cells (Tfh) (Cre$^+$: $N = 5$; Maf$^{\Delta B}$: $N = 8$) and the coefficient and P value ($p < 0.0001$) from the Pearson correlation **g** Pseudocolor plots illustrating plasmablasts (PBs) gated on live cells and bar graphs showing total PB cell counts ($p = 0.0027$). **h** Pseudocolor plots illustrating antibody secreting cells (including both PBs and plasma cells) gated on live cells and bar graphs showing total antibody secreting cells counts. ($p = 0.26$) Data show mean ± SEM (**a**–**h**). Statistical analysis: unpaired two-tailed Mann–Whitney tests (**a**, **d**, **e**, **g**, **h**) or ANOVA test using Tukey's correction for multiple comparisons (**b**, **c**) *$p < 0.05$, **$p < 0.01$, ***$p < 0.001$, ns not significant. Source data are provided as a Source Data file.

activation and proliferation. Thus, we examined the proliferative response of B cells in vitro following 4 days of stimulation with anti-IgM Abs, LPS, or anti-CD40 Abs in the presence of IL-4 and IL-5. No change in the proliferation index was observed in all conditions for the overall B cell population (Supplementary Fig. 4a), indicating similar number of divisions in mutant and control proliferating B cells. However, when gated specifically, CD138$^+$ PBs from Maf$^{\Delta B}$ B-cell cultures showed higher proliferation index following both LPS and anti-CD40Abs +IL-4 and IL-5 stimulation (Supplementary Fig. 4b). In addition, the division index, which represents the average number of divisions of all (dividing and non-dividing) cells, was higher for Maf$^{\Delta B}$ B cells stimulated with LPS, but not with other stimulatory conditions (Supplementary Fig. 4a). This indicates that Maf deficiency allows a larger number of B cells (46.24 ± 7.8% in Maf$^{\Delta B}$ *vs* 25.48 ± 2.5% in control, $p = 0.0079$) to enter the cell cycle in response to LPS and it promotes more proliferation once cells differentiate into PBs.

https://doi.org/10.1038/s41467-024-52224-6

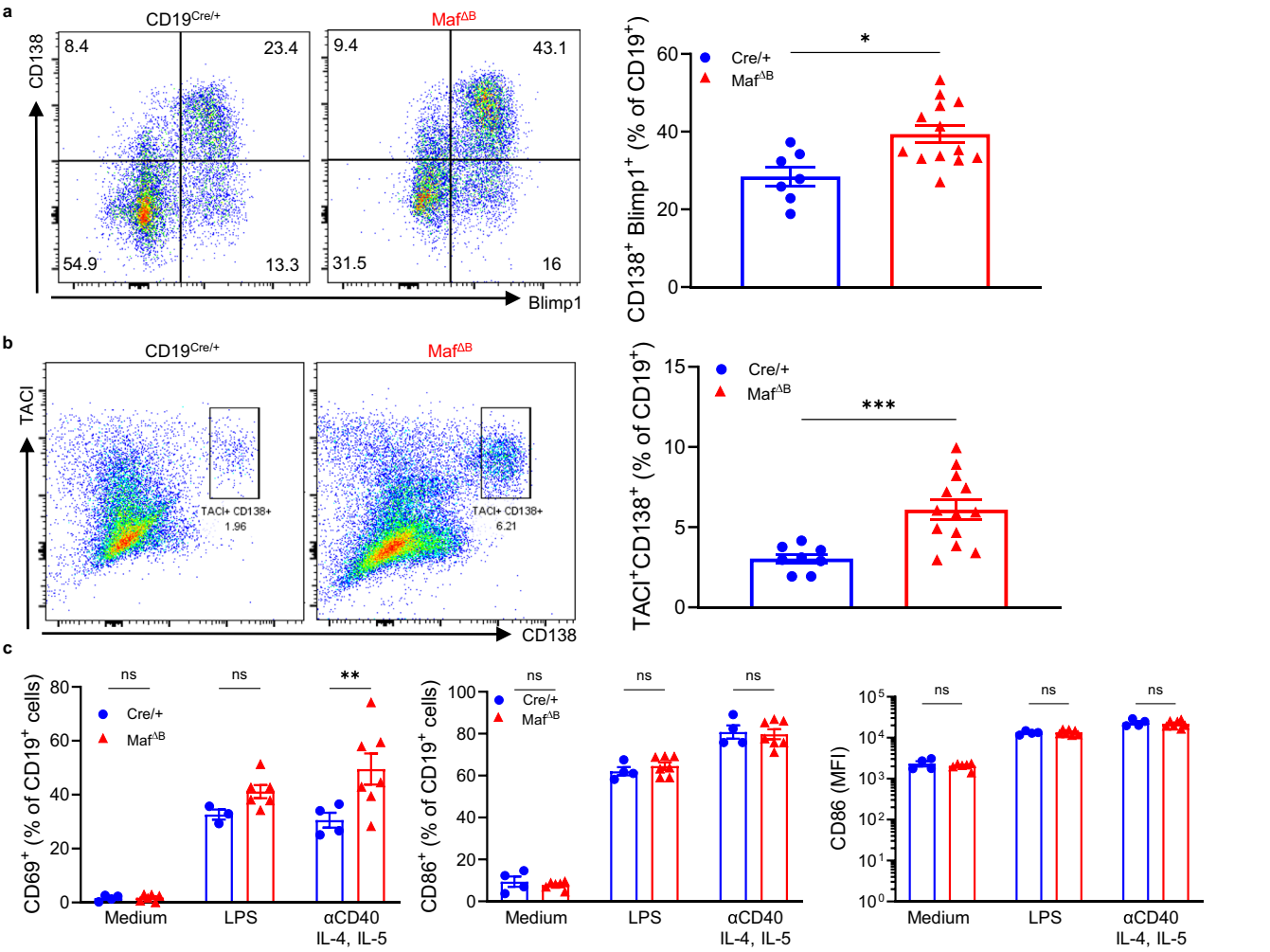

Fig. 2 | In vitro stimulated B cells from Maf$^{\Delta B}$ mice exhibit enhanced differentiation into plasmablasts. Analysis of in vitro-stimulated B cells from CD19$^{Cre/+}$ and Maf$^{\Delta B}$ mice. **a** Pseudocolor plots and bar graphs showing percentages of CD138$^+$Blimp1$^+$ PB cells of CD19$^+$ live cells after LPS stimulation (Cre$^+$: $N = 7$; Maf$^{\Delta B}$: $N = 13$, $p = 0.011$). **b** Pseudocolor plots and bar graphs showing percentages of CD138$^+$TACI$^+$ PB cells of stimulated CD19$^+$ live cells (Cre$^+$: $N = 8$; Maf$^{\Delta B}$: $N = 13$, $p = 0.0009$). **c** Bar graphs showing percentages of CD69$^+$ cells, of CD86$^+$ cells, and CD86 mean fluorescence intensity (MFI) gated on live CD19$^+$ B cells 3 days after stimulation. (Cre$^+$: $N = 3$–4; Maf$^{\Delta B}$: $N = 6$-7). Data show mean ± SEM (**a**–**c**). Statistical analysis: unpaired two-tailed Mann–Whitney tests (**a**, **b**) or one-way ANOVA test using Tukey's correction for multiple comparisons (**c**). $^{**}p < 0.01$, $^{***}p < 0.001$, ns not significant. Source data are provided as a Source Data file.

We next investigated the proliferative B cell response to T-dependent antigen in vivo. For this, we immunized control CD19$^{Cre/+}$ and Maf$^{\Delta B}$ mice with NP-CGG in alum and 3 days later injected the mice with the thymidine analog 5-Ethynyl-2'-deoxyuridine (EdU) to label cells actively proliferating. Two days later, the mice were injected with 5-bromodeoxyuridine (BrdU) to label currently proliferating cells and analyzed 1 h thereafter (Fig. 4a). Both EdU and BrdU have a short half-life in vivo, with a bioavailability lasting only one hour. Thus, this time frame of immunization and DNA labeling allows to observe the early phase of B-cell activation and blasting, the EF-PB cell production, and the initiation of GC reactions[28–32]. NP$^+$ cells were separated according to CD138 and GL7 expression to identify CD138$^-$GL7$^+$ GC B cells, CD138$^+$ EF-PBs, and CD138$^-$GL7$^-$ activated B cells specific for NP antigen. Five days after immunization, and in agreement with earlier observations (Fig. 3a–c), Maf$^{\Delta B}$ mice harbored higher numbers of NP-specific PBs and GC B cells relative to control mice (Fig. 4b). Antigen-specific B cell subsets were further analyzed for EdU and BrdU incorporation to identify the following proliferative and non-proliferative cells: EdU$^-$BrdU$^-$ cells that were not proliferating either on day 3 or day 5; EdU$^+$BrdU$^-$ cells that were in the S phase at day 3 but not on day 5; EdU$^+$BrdU$^+$ cells that were in the S phase both at days 3 and 5; and EdU$^-$BrdU$^+$ cells that were not proliferating on day 3 but were in the S phase on day 5 (Fig. 4c). This analysis detected no differences in the proliferation of NP-specific activated B cells between control and Maf$^{\Delta B}$ mice (Fig. 4c). There was also no difference in the frequency of proliferative PBs and GC NP$^+$ B cells early on (day 3, EdU$^+$ cells) in the response (Fig. 4c). In contrast, there was a marked increase in the frequency of proliferating (BrdU$^+$EdU$^-$) NP-specific EF-PB cells at day 5, and a trend to an increase in GC B cell proliferation at the same time (Fig. 4c). These data indicate that Maf does not regulate early events of B-cell activation and blasting, but it restrains the proliferation and expansion of antigen-specific PBs and GC B cells after the initiation of the full response.

We next examined in depth GC B cells to determine if Maf regulates the distribution of B cells in the dark zone (DZ) and the light zone (LZ). In line with the increase of GC B cell proliferation previously observed, we found a higher ratio of CXCR4^{high}CD86^{low} DZ cells to CXCR4^{low}CD86$^+$ LZ cells in Maf$^{\Delta B}$ mice compared to control mice (Fig. 4d). This finding was not due to differences in cell apoptosis (Fig. 4e). To further elucidate Maf involvement in controlling B-cell proliferation in the GC, we measured EdU incorporation and 7AAD staining (i.e., DNA content) in NP$^+$ (i.e., antigen-specific) GC B cells

https://doi.org/10.1038/s41467-024-52224-6

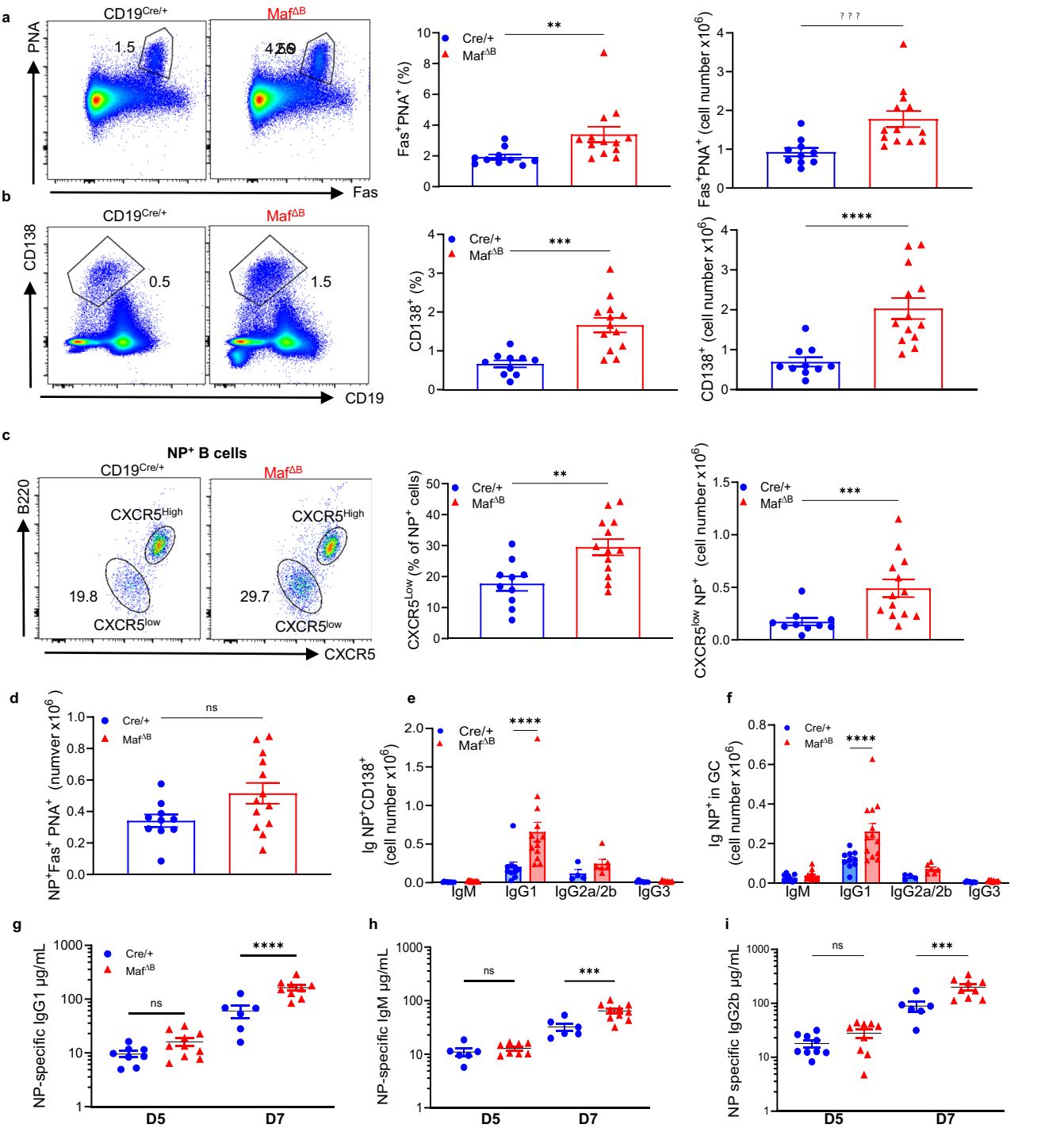

Fig. 3 | Maf$^{\Delta B}$ mice mount stronger GC reaction and extrafollicular PB generation following T-dependent immunization. B cell response to NP-CGG in CD19$^{Cre/+}$ and Maf$^{\Delta B}$ mice. **a** Pseudocolor plots of GC B cells according to PNA-binding and Fas expression gated on live B220$^+$ B cells in spleen at day 7 after immunization with NP-CGG in alum; bar graphs showing percentages (of B220$^+$ cells, $p = 0.0015$ and numbers of Fas$^+$PNA$^+$ GC B cells ($p = 0.0005$). **b** Pseudocolor plots of plasmablast (PB) gated on live cells; bar graphs showing total CD138$^+$ PB and Fas$^+$ PNA$^+$ GC cell counts. **c** Pseudocolor plots of NP-specific extra-follicular (EF-PB) cells; bar graphs showing percentages ($p = 0.0068$) and total NP$^+$ EF-PB cells (CXCR5^{low}, $p = 0.0006$). **d** Bar graphs showing number of NP$^+$(i.e., NP-binding) Fas$^+$PNA$^+$ GC B cells at day 7. **e**, **f** Bar graphs showing Ig isotype-positive cell numbers among NP$^+$ CD138$^+$ PB cells ($p < 0.0001$) **e** and GC B cells ($p < 0.0001$) **f** at day 7. Scatter dot plots showing serum NP-specific **g** IgG1($p < 0.0001$) **h** IgM ($p = 0.0008$) and **i** IgG2b ($p = 0.0006$) antibodies measured at days 5 and 7 after immunization. **a**–**d**: Cre$^+$: $N = 10$; Maf$^{\Delta B}$: $N = 13$; **e**–**i** Cre$^+$: $N = 4$-10, Maf$^{\Delta B}$: $N = 6$–14. Data show mean ± SEM and Statistical analysis: unpaired two-tailed Mann–Whitney tests (**a**–**d**) or ANOVA test using Tukey's correction for multiple comparisons (**e**–**i**). $^{**}p < 0.01$, $^{***}p < 0.001$, ns not significant. Source data are provided as a Source Data file.

10 days after NP-CGG immunization and 1 h after EdU injection. This analysis distinguished non-proliferating NP$^+$ GC B cells in GO/G1 phase (EdU$^-$7AAD$^-$), cells in early S phase (EdU$^+$7AAD$^-$), cells in late S phase (EdU$^+$7AAD$^+$), and cells in G2/M phase (EdU$^-$7AAD$^+$). The analysis uncovered a large increase of cells in late S phase of the cell cycle among DZ B cells from Maf$^{\Delta B}$ mice compared to controls, which correlated with an increase of cells in G2/M phase in the LZ (Fig. 4f). Despite the increased cell proliferation in the GC of Maf$^{\Delta B}$ mice, the

https://doi.org/10.1038/s41467-024-52224-6

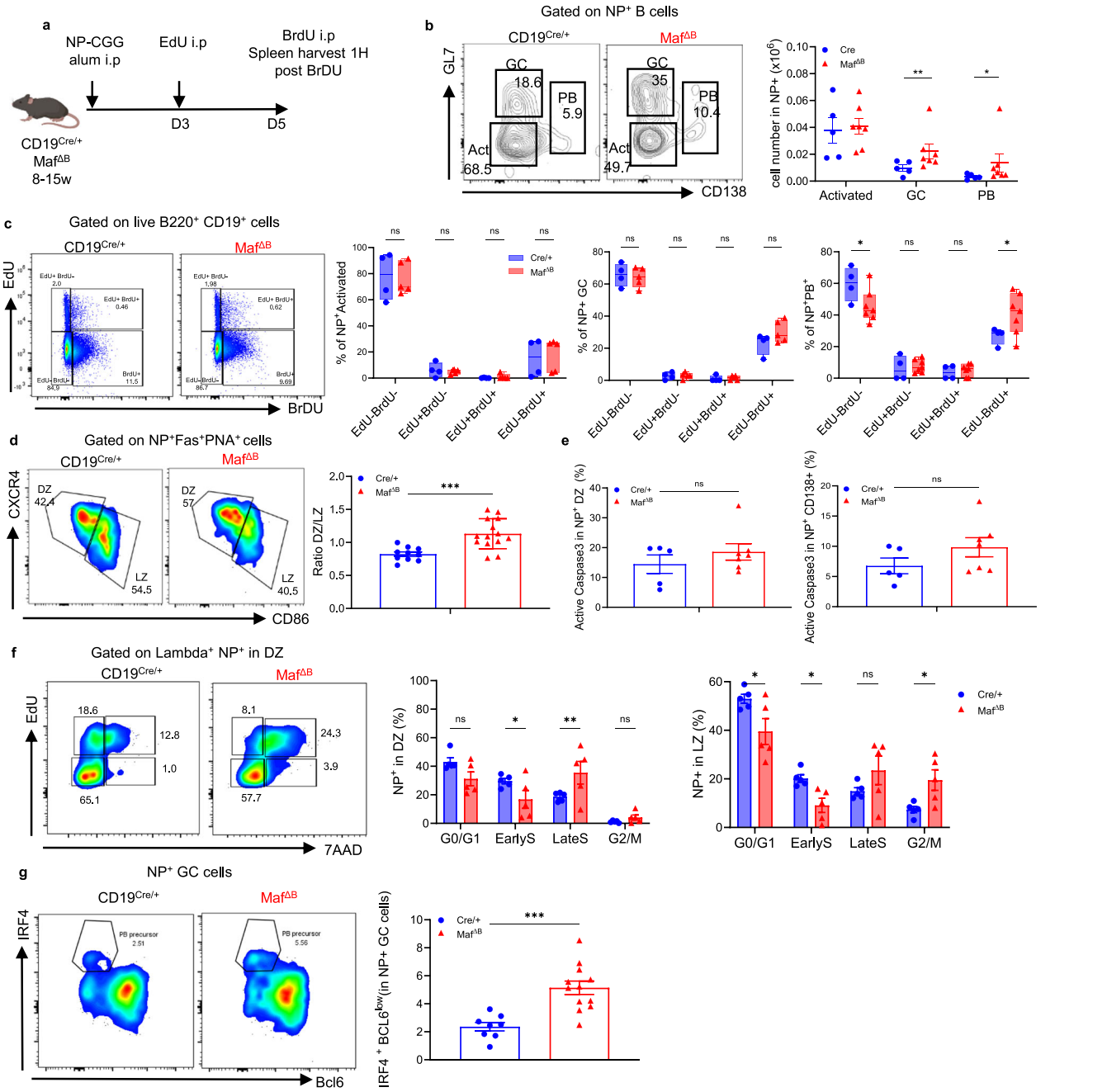

Fig. 4 | Maf regulates B cell proliferation in GC B cells and plasmablasts during T-dependent responses. a Scheme of experiment. After immunization with NP-CGG-in alum, CD19$^{Cre/+}$ ($N = 4$) and Maf$^{\Delta B}$ mice ($N = 5$–7) were injected with EdU on day 3 and with BrdU on day 5 and were analyzed 1 h after the BrdU injection. **b** Countour plots illustrating NP-specific CD19$^+$ B cells at day 5 post-immunization and bar graphs showing numbers of NP-specific activated, PB ($p = 0.0088$), and GC ($p = 0.036$) CD19$^+$ B cells. **c** Pseudocolor plots of EdU and BrdU in B220$^+$CD19$^+$ B cells at day 5 post-immunization and bar graphs showing percentages of each EdU/BrdU subset in NP-binding activated, PB (Edu-BrdU-, $p = 0.0107$; Edu-BrdU+, $p = 0.0123$) and GC B cells. **d** Pseudocolor plots illustrating NP$^+$ (i.e., NP-binding) Fas$^+$PNA$^+$ GC B cells at day 7 post-immunization. Bar graphs showing the ratio of the number of dark zone (DZ), and light zone (LZ, Cre$^+$: $N = 10$; Maf$^{\Delta B}$: $N = 14$, $p = 0.0005$. **e** Bar graphs showing percentages of active caspase 3 positive cells in NP$^+$ DZ cells and CD138$^+$ PBs at day 7 post-immunization. Cre$^+$: $N = 5$; Maf$^{\Delta B}$: $N = 7$. **f** CD19$^{Cre/+}$ and Maf$^{\Delta B}$ mice were immunized with NP-CGG in alum and, after 10 days, mice were injected with EdU and analyzed 1h thereafter. Pseudocolor plots illustrating CD19$^+$NP$^+$ GC DZ B cells and bar graphs showing cells in G0/G1 (EdU$^-$7AAD$^-$, NP$^+$LZ, $p = 0.016$), early S phase (EdU$^+$7AAD$^-$, NP$^+$DZ, $p = 0.038$; NP$^+$LZ, $p = 0.032$), late S phase (EdU$^+$7AAD$^+$), NP$^+$DZ, $p = 0.0082$), and G2/M (EdU$^-$7AAD$^+$, NP$^+$LZ, $p = 0.02$) among NP-specific DZ and LZ B cells. Cre$^+$: $N = 5$; Maf$^{\Delta B}$: $N = 5$. **g** Dot plots of NP$^+$ GC B cells (gated as CD19$^+$ B220$^+$CD38^{low}GL7$^+$) at day 12 post-immunization with NP-CGG in alum and bar graphs showing percentages of IRF4$^+$BCL6^{low} PB precursor cells among NP-specific GC B cells. Cre$^+$: $N = 8$; Maf$^{\Delta B}$: $N = 12$, $p = 0.0003$. Bar graphs represent mean ± SEM (**b**, **d**–**g**) and box plots indicate median (middle line), 25th, 75th percentile (box) and min/max (whiskers). Statistical analysis: unpaired two-tailed Mann–Whitney tests and ANOVA using Fisher's Least Significant Difference (LSD) test for multiple comparisons. *$p < 0.05$, **$p < 0.01$, ***$p < 0.001$, ns not significant. Source data are provided as a Source Data file.

number of NP$^+$ cells was similar to that in controls (Fig. 3d). To reconcile these data, we hypothesized that Maf-deficiency leads to an accelerated differentiation of antigen-specific GC B cells into PBs/PCs. To identify PC precursors in GCs[33], we examined IRF4 and BCL6 expression and found a large increase of the IRF4$^+$BCL6^{low} cell population among LZ B cells of Maf$^{\Delta B}$ mice compared to controls, supporting our hypothesis (Fig. 4g). Taken together, these data show that Maf deficiency results in an acceleration of the cell cycle in GC B cells and increases the development of IRF4$^+$ PB/PC precursors, leading to a heightened PB output. This indicates that Maf inhibits B cell progression into the cell cycle and subsequent differentiation to PC precursors.

Affinity mutation is a tightly regulated process that occurs in the germinal center. To explore this aspect, we performed NP_4 (high affinity) and NP_{36} (low affinity) IgG1 ELISA measurements as previously described[28]. On day 7 post-immunization, we observed a trend to a decrease in the NP_4/NP_{36} ratio in Maf$^{\Delta B}$ mice suggesting that the increase in anti-NP IgG1 in the absence of Maf mostly corresponds to low-affinity Ig production (Supplementary Fig. 4c). However, on days 12 and 28, this difference was not present, and the ratio increased equally in both groups indicating that the overall production of high-affinity antibodies is not affected by the deletion of Maf in the GC.

Maf does not contribute to the IgG$^+$ B-cell memory response

The changes in B-cell proliferation observed in Maf$^{\Delta B}$ mice suggested that Maf could participate also in the generation of GC-derived memory B cells. To investigate this, we immunized control and Maf$^{\Delta B}$ mice with NP-CGG in alum and, ten days later, we injected the mice with EdU and analyzed them at days 12 and 28 to identify the fate of the GC B cells (Fig. 5a). As observed before, EdU$^+$ B cells were increased at day 12 within the CD138$^+$ NP$^+$ PBs of Maf$^{\Delta B}$ mice relative to controls (Fig. 5b). There was also a slight increase of EdU$^+$ B cells within the IgM$^+$ memory B cells (CD138$^-$CD38$^+$IgM$^+$). However, there was no difference in the frequency of EdU$^+$ cells among switched IgG$^+$ memory B cells identified as CD138$^-$CD38$^+$ and IgG1$^+$ or IgG2a/2b$^+$ (Fig. 5c). Frequency and absolute numbers of CD38$^+$lambda$^+$ B cells were also similar in control and Maf$^{\Delta B}$ mice 28 days after immunization (Fig. 5d). We next examined the distribution of memory B cell subsets expressing CD80 and PDL2[34] within both switched and unswitched Ag-specific B cell populations identified as IgM$^+$CD38$^+$lambda$^+$ or IgG$^+$CD38$^+$lambda$^+$[35,36]. There was no difference between control and Maf$^{\Delta B}$ mice in the frequency of double positive CD80$^+$PDL2$^+$ (Fig. 5e, f). However, there was a mild but significant increase in the percentage of single-positive CD80$^-$PDL2$^+$ cells in Maf$^{\Delta B}$ mice in both switched and unswitched memory compartments. Altogether, these data show that Maf does not significantly regulate the formation of committed memory B cells arising from the GC.

Maf promotes long-lived plasma cells

Although it is not clear whether long-lived plasma cells represent the final differentiation stage of short-lived PBs or whether they belong to separate cell lineages, we sought to examine these populations 28 days after NP-CGG immunization. In the spleen, there was no significant difference in the number of lambda$^+$CD138$^+$ PBs (Fig. 6a). To discriminate between PBs and PCs by flow cytometry, we distinguished cells for surface lambda (SLambda) and intracellular lambda (ICLambda) expression[37]. The percentage of the ICLambda$^+$SLambda$^-$ PC fraction was decreased in the spleen of Maf$^{\Delta B}$ mice compared to control mice (Fig. 6b), suggesting that Maf could modulate PC fate contributing either to the differentiation of PBs into PCs or the migration of PCs to the BM. To discriminate these options, we analyzed PBs and PCs in BM tissue. There was no significant difference in total CD138$^+$ antibody secreting cells (ASCs) or in the frequency of lambda$^+$ ASCs in the BM of Maf$^{\Delta B}$ and control mice (Fig. 6c, d). Nevertheless, there was a significant decrease in the proportion of ICLambda$^+$SLambda$^-$ cells within the kappa$^-$CD138$^+$ cell subset in Maf$^{\Delta B}$ mice compared to controls (Fig. 6e), and this correlated with a (non-significant) trend to reduced NP-specific IgG1 Abs in sera (Fig. 6f). To better explore the heterogeneity of lambda$^+$ ASCs, we employed a flow cytometry protocol that leverages differential expression of CD19 and B220 to identify different PC populations[38] This protocol enabled us to discriminate CD138$^+$kappa$^-$cells in the BM into CD19$^+$B220$^+$ proliferating PBs, CD19$^+$B220$^-$ early PCs, and CD19$^-$B220$^-$ mature resting PCs. This analysis shows a decreased frequency of mature resting PCs and an increased frequency of early PCs in Maf$^{\Delta B}$ mice (Supplementary Fig. 4d), suggesting that Maf does not play a role in the transition between PBs and PCs but rather in the establishment of mature PCs. These data suggest that Maf contributes to the establishment and possibly the maintenance of long-lived PCs.

Dissecting the molecular contribution of Maf by scRNA-seq analyses

To gain insight into the molecular changes that occurred in Maf$^{\Delta B}$ mice during the TD immunization response, we performed single-cell RNA sequencing (scRNAseq) of B cells isolated 7 days after NP-CGG immunization. After removing contaminating cells (T cells and macrophages), we resolved 16,904 B cells into 17 clusters (Fig. 7a). These were identified as such: four clusters of follicular B cells (C0, 1, 2, and 4), one cluster of marginal zone B cells (C11), five clusters of GC cells (C5, 7, 10, 12, and 16), two clusters of memory B cells (C8 and C14), two clusters of lambda$^+$ cells (C9, *Iglc1*, and C15 *Iglc2*), one atypical cluster of B cells expressing *Lars2* (C3), one cluster with an upregulation of type I-IFN signature (C6), and one cluster of PBs (C13) (Fig. 7b). In control mice, *Maf* expression was relatively low in most B-cell clusters with higher expression in C0 (FO1), C4 (F04 Iglc1+), C6 (IFN), and C7 (Fig. 7c). As expected, *Maf* expression was no longer detectable in Maf$^{\Delta B}$ mice (Fig. 7d and Supplementary Fig. 5a). Except for an important reduction of the C3 cluster in Maf$^{\Delta B}$ (KO) mice, there were no major changes in the distribution of the different clusters between WT and KO B cells.

Next, we used recent public data and computational analysis pipelines[39–41] to extend our analysis on GC clusters. Based on this, we assigned Cluster 5 to pre-GC cells that are mostly characterized by the expression of *Il4i1, Mif, Npm1* and *Bcl2a1b* (Fig. 7b). Of the remaining four clusters of GC cells, C16 and C12 likely belonged to the DZ because of their high expression of genes involved in cell proliferation such as *Mki67*, *Birc5*, *Hist1h1b*, and *Gclm*. To quantitatively assess inferences of mitotic status and confirm assignment of germinal center-related clusters, we used previous cell cycle gene signature[39,42] and trajectory analysis through RNA velocity[43] (Fig. 7e). As expected, G1/S and G2/M signatures score were significantly elevated in C16 and C12 with a homology of trajectory comparing to clusters C0 (resting B cells), C7 and C10 (Supplementary Fig. 5b). Upon examining the LZ and DZ gene signature score[39], we found that C12 and C16 corresponded to DZ cells, while C7 were most likely LZ cells (Fig. 7f and Supplementary Data 1). Interestingly, C10 exhibited an upregulation of both gene signatures and displayed a strong developmental relationship in cell trajectory with C7.

To confirm this cluster assignment, we used topic modeling[39] to capture composite states in GC clusters relative to resting B cells in Cluster 0 and PBs in C13. Topic modeling identified a common mitotic signature (topic 8, *Mki67*, *Birc5*, *Aicda* and topic 5, *Npm1*, *Eif5a*, *Eif4a1*, *Hspd1*) in C12 and C16 consistent with DZ features (Supplementary Fig. 5c and Supplementary Data 2). As a result, we categorized C16 within DZ1 and assigned C12 to DZ2. Topic 6, enriched in C5, C7 and C10, showed upregulation of markers for LZ and DZ transition *(Nr4a1, Cd83, Myc, Bhlhe40, Il21r and Rel*[44–46]), placing C7 in LZ1 and C10 in LZ2. Cluster 10 cells (LZ2) expressed genes (*Bcl11a*, *Ets1, Ikzf3, Tcf4* and *Mef2c)* linked to signaling activation, indicating involvement in Ag selection and T cell interaction[47,48].

https://doi.org/10.1038/s41467-024-52224-6

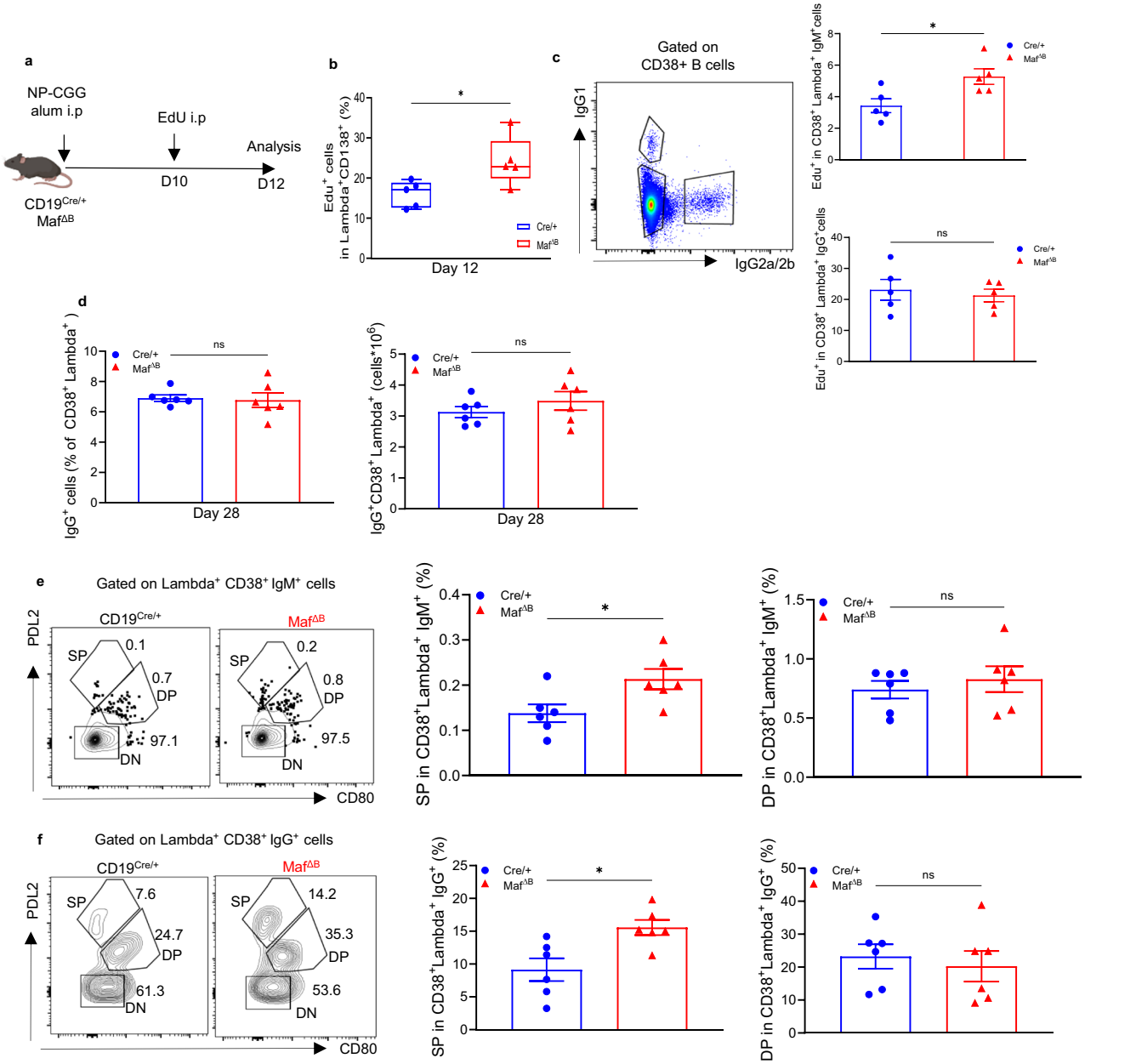

Fig. 5 | Maf does not contribute to B cell memory formation. Analysis of memory B cell response to NP-CGG in CD19$^{Cre/+}$ and Maf$^{\Delta B}$ at day 12 (**a**–**c**, Cre^{+}: $N = 5$; Maf$^{\Delta B}$: $N = 5$) and day 28 post-immunization (**d**–**f**, Cre^{+}: $N = 6$; Maf$^{\Delta B}$: $N = 6$). **a** Mice were immunized i.p with NP-CGG in alum. On day 10 after immunization, mice were injected i.p with EdU and then analyzed on days 12 and 28 after immunization. **b** Box plots showing percentages of EdU^{+} cells among NP-binding CD138^{+}lambda^{+} cells ($p = 0.039$) **c** Pseudocolor plots illustrating CD38^{+} non-GC B cells and bar graphs showing percentages of EdU^{+} cells in CD38^{+}IgG^{-} B cells ($p = 0.031$) and CD38^{+}IgG^{+} (including IgG1 and IgG2a/b, $p = 0.73$) B cells. **d** Box plots showing percentages of IgG^{+} cells (including IgG1 and IgG2a/b, $p = 0.48$) in CD38^{+}lambda^{+} B cells and IgG^{+}CD38^{+}lambda^{+} B cell numbers ($p = 0.48$). **e** Dot/countour plots illustrating CD38^{+}lambda^{+}IgG^{-} B cells and bar graphs showing percentages of single-positive (SP, CD80^{-}PDL2^{+}, $p = 0.04$) and double-positive (DP, CD80^{+}PDL2^{+}, $p = 0.36$) subsets in CD38^{+}lambda^{+}IgM^{+} B cells. **f** Countour plots of CD38^{+}lambda^{+}IgG^{+} (IgG1 and IgG2a/b) B cells and bar graphs showing percentages of CD80/PDL2 SP ($p = 0.01$) and DP subsets ($p = 0.56$) in CD38^{+}lambda^{+}IgG^{+} B cells. Bar graphs represent mean ± SEM (**c**–**f**) and box plots indicate median (middle line), 25th, 75th percentile (box) and min/max (whiskers). Statistical analysis: unpaired two-tailed Mann–Whitney tests. *$p < 0.05$, **$p < 0.01$, ***$p < 0.001$, ns not significant. Source data are provided as a Source Data file.

To uncover the gene-regulatory network modulated by the Maf transcription factor, we performed gene differential expression (DEG) across the different B cell clusters between Maf$^{\Delta B}$ and control mice. The analysis of DEG in the naïve and activated B cells clusters (C0, 1, 2 and 4) and pre-GC cells (C5) revealed very limited changes in gene expression between control and Maf$^{\Delta B}$ mice (C0: 27 DEGs, C1: 23, C2: 19, C4: 24, and C5: 22). These data support that Maf has a minimal (or redundant) role in early maturation and activation of B cells. Among the original B cell clusters of GC cells, the number of DEGs increased to 461 for C16/DZ1 and 72 for C12/DZ2 (Fig. 8a, b). Pathway analysis revealed upregulation of genes involved in DNA replication and cell proliferation such as *Mki67*, *Cenpf*, *Hist1h2ae*, *Birc5*, and *Cks2* (Supplementary Fig. 5d). GSEA study revealed that an important set of genes regulated by Maf are involved in cellular metabolism, transporter activity, and mitochondrial proteins (Fig. 8c, d), mechanisms recently described as crucial in controlling the GC reaction[49,50]. The C7/LZ1 cluster from Maf$^{\Delta B}$ mice displayed 22 DEGs with the upregulation of two key factors in the GC reaction, *Nr4a1* and *Myc* (Fig. 8b, e). The

https://doi.org/10.1038/s41467-024-52224-6

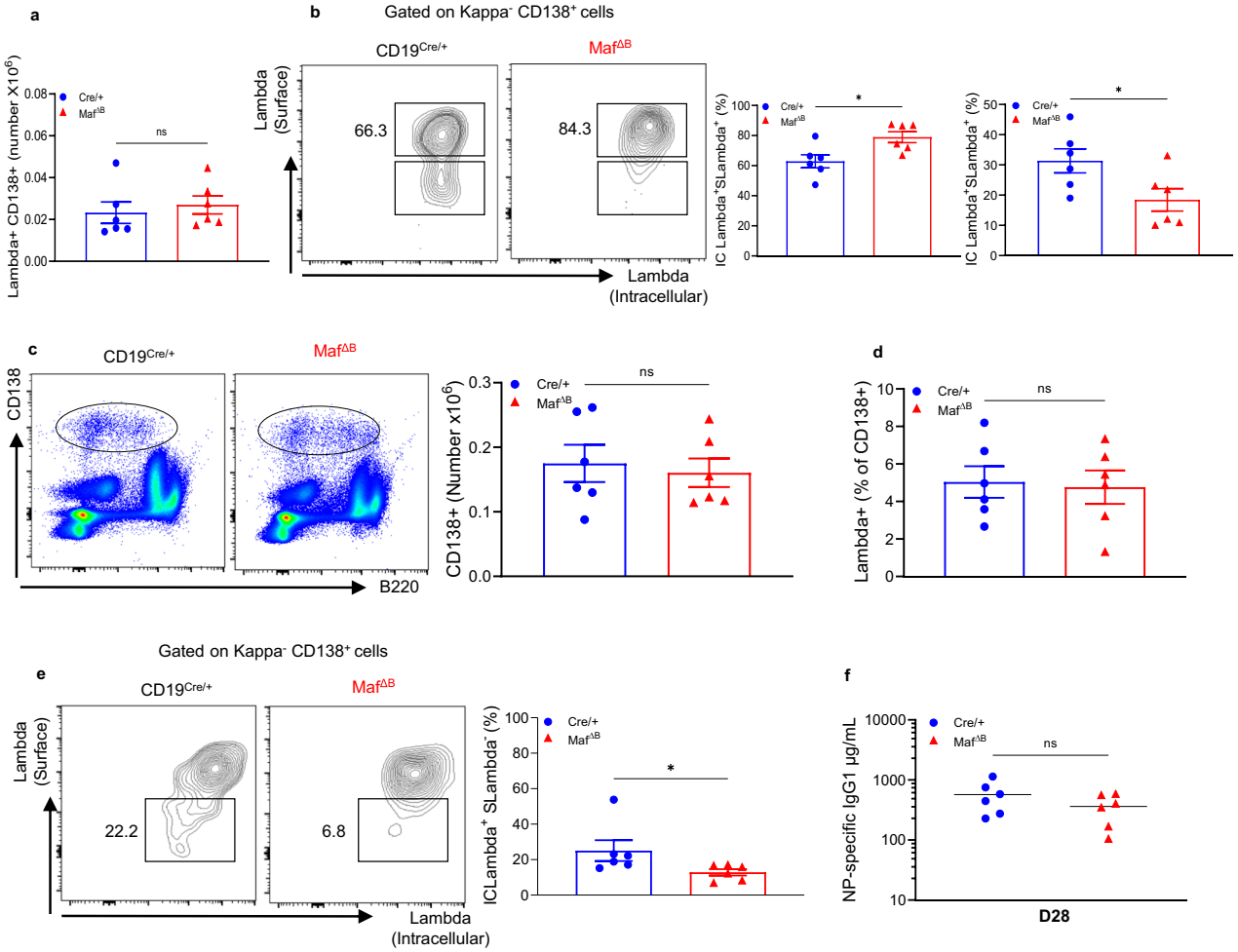

Fig. 6 | Maf$^{\Delta B}$ mice generate reduced numbers of long-lived plasma cells. Analysis of plasma cells in response to NP-CGG immunization. CD19$^{Cre/+}$ ($N = 6$) and Maf$^{\Delta B}$ ($N = 6$) mice were immunized i.p with NP-CGG in alum and analyzed 28 days after immunization. **a** Bar graphs showing total number of NP-specific lambda$^+$CD138$^+$ cells in spleen ($p = 0.3$). **b** Dot plots illustrating kappa$^-$CD138$^+$ ASCs in spleen according to surface (S) and intracellular (IC) lambda expression and bar graphs showing percentage of Slambda$^+$ IClambda$^+$ cells ($p = 0.015$) and of surface Slambda$^-$IClambda$^+$ ($p = 0.041$) cells among kappa$^-$CD138$^+$ cells of spleen. **c** Pseudocolor plots illustrating CD138$^+$ bone marrow (BM) cells and bar graphs showing total cell numbers in BM ($p = 0.5$). **d** Bar graphs showing percentage of lambda$^+$ cells in the CD138$^+$ compartment of BM ($p = 0.9$). **e** Countour plots illustrating kappa$^-$CD138$^+$ cells in BM bar graphs showing percentages of Slambda$^-$IClambda$^+$ cells ($p = 0.017$) among kappa$^-$CD138$^+$ cells in BM. **f** Distribution of serum NP-specific IgG1 antibodies ($p = 0.3$). Data show mean ± SEM (**a**–**f**). Statistical analysis: unpaired two-tailed Mann–Whitney tests. *$p < 0.05$, **$p < 0.01$, ns not significant. Source data are provided as a Source Data file.

increased *Myc* mRNA in B cell from Maf$^{\Delta B}$ mice was confirmed at the protein level by flow cytometry in NP$^+$ LZ cells gated as CD38^{low}Fas$^+$ and NP$^+$CD86$^+$CXCR4^{low} (Fig. 8f), suggesting that Maf deletion might positively regulate the Myc-dependent signature during immunization.

Pathway and GSEE analyses revealed an enrichment in genes involved in the metabolic pathway, transporter activity, and oxydoreductase mechanisms in GC clusters (Fig. 8c, d). These observations were extended by analyzing the gene signature score associated to metabolic pathways. The OXPHOS pathway was significantly upregulated in DZ1 (C16) and LZ2 (C10) from Maf$^{\Delta B}$ mice whereas glycolysis and fatty acid oxidation (FAO) pathways were slightly reduced in C16/DZ1 of Maf$^{\Delta B}$ mice (Fig. 8g). To assess consequences of Maf deletion on mitochondrial functions, we conducted an analysis of mitochondrial activities in GC B cells after 7 days of NP-CGG immunization using two MitoTracker™ Dyes, Mitotracker FeepRed FM to measure mitochondrial membrane potential and MitoSox to measure reactive oxygen species (ROS)[51] Whereas the mitochondrial membrane potential was similar in GC B cells from Maf$^{\Delta B}$ and control mice, we observed a significant increase in the percentage of MitoSox-positive (ROS-producing) cells in GC B cells from Maf$^{\Delta B}$ mice (Supplementary Fig. 5e, f). This suggests that Maf regulates mitochondrial activities by modulating ROS production.

Finally, we analyzed the C13 cluster characterized by an upregulation of *Igh* genes, *Xbp1*, *Jchain*, and *Prdm1* and assigned to PBs. 59 DEGs were found in C13 between Maf$^{\Delta B}$ and control mice (Supplementary Fig. 5g). Among the DEGs, *Igha*, *Ighg1*, *Iglc1*, and *Iglc2* were significantly up-regulated in Maf$^{\Delta B}$ cells, confirming that KO PB cells are enriched in class-switched NP-specific cells. We identified several up-regulated genes in Maf$^{\Delta B}$ B cells that have been described as important regulators of GC development and PC differentiation, such as *Tcf4* (E2-2)[48,52], *Tram2* (Blimp1 target)[20] and *Sub1* (Irf4 target) encoding PC4[53,54].

Taken together, these results demonstrate that Maf has a B-cell intrinsic function that restrains the generation of GC B cells and newly differentiated PBs by controlling cell proliferation and metabolism.

Discussion

In this report, we demonstrate that the transcription factor Maf functions intrinsically in B cells to dampen the development of marginal zone B cells, germinal center B cells, and PBs in naive mice. Following a T-cell-dependent immunization, Maf restrains extra-follicular PB

https://doi.org/10.1038/s41467-024-52224-6

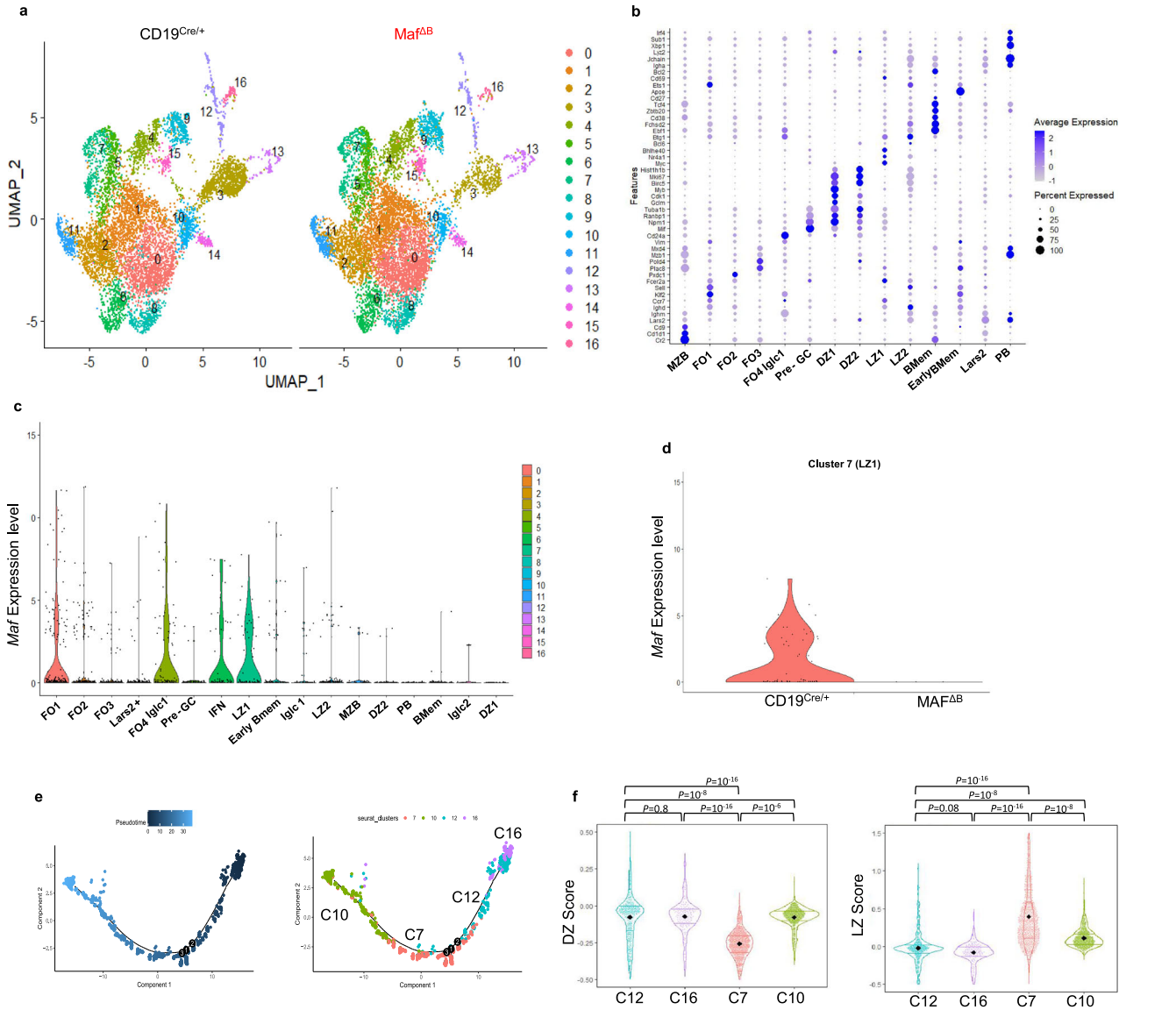

Fig. 7 | Single cell RNAseq analysis of B cells responding to NP-CGG immunization. CD19$^{Cre/+}$ and Maf$^{\Delta B}$ mice were immunized i.p with NP-CGG in alum. Seven days after immunization, splenic B cells were isolated using negative selection. ScRNAseq was performed on B cells pooled from two individual mice of each strain. **a** UMAP projections of scRNA-seq profiles of 16,904 B cells from the two groups of mice. Clusters in the UMAP plots are color coded according to different cell populations. **b** Mean expression of selected marker genes in each B cell cluster. Color intensity denotes average gene expression, whereas dot size represents the percentage of cells expressing the gene. **c** Violin plots of *Maf* gene expression in cells of each cluster in integrated data. **d** Violin plot of *Maf* expression in cluster 7 (LZ1) of CD19$^{Cre/+}$ and Maf$^{\Delta B}$ mice. **e** Pseudotime analysis of GC B cell clusters trajectories analyzed using Slingshot R package. Analysis was performed on B cells in clusters C7, C10, C12 and C16. **f** Violin plots of the distribution of dark zone (DZ) and light zone (LZ) gene signature scores (based on ref. 39, Supplementary Data 1) in clusters 7, 10, 12 and 16. Statistical analysis: ANOVA test using Tukey's correction for multiple comparisons.

generation and B-cell expansion within the germinal center. Our findings indicate that Maf does not regulate the early events of B-cell activation and blasting, but it restrains the proliferation and expansion of antigen-specific PBs and germinal center B cells after the initiation of the full response. Germinal center B cells that lack Maf show an acceleration of the cell cycle, leading to an increase in the development of IRF4^{+} PB/plasma cell precursors and heightened PB output. Our data show that Maf has a B-cell intrinsic function and restrains the generation of germinal center B cells and newly differentiated PBs mostly through control of cell proliferation and metabolic processes.

A B cell-specific Maf deficiency did not influence the TI-2 T cell independent antibody response but resulted in a heightened TD response at both the extra-follicular sites and within the GC. This led to a dramatic and significant increase of antigen-specific IgG1 antibodies in the first few days after immunization. Our data also revealed an increase in PB differentiation in response to LPS stimulation without any strong modification of B-cell activation. This was likely accounted for, at least in part, by higher numbers of marginal zone B cells in Maf$^{\Delta B}$ mice, given that MZB cells are hyper-responsive to LPS[55]. However, an increase in PB generation was also observed in vitro with total splenic B cells in the presence of T-cell derived signals (CD40L, IL-4 and IL-5) (Fig. 2) indicating that Maf generally restrains PB differentiation in a B-cell intrinsic manner. The PB increase in Maf$^{\Delta B}$ mice was not due to changes in Blimp1 expression, but rather appeared to be related to the regulation of B-cell proliferation. Based on BrdU incorporation data, Maf was observed to regulate the proliferation of antigen specific PBs, but not that of activated B cells. Interestingly, a B cell-restricted deletion of Maf did not increase B cell proliferation generally in all B cells in vitro, but only increased proliferation in differentiated PBs. Indeed, newly generated Maf-deficient PBs displayed increased BrdU/EdU

https://doi.org/10.1038/s41467-024-52224-6

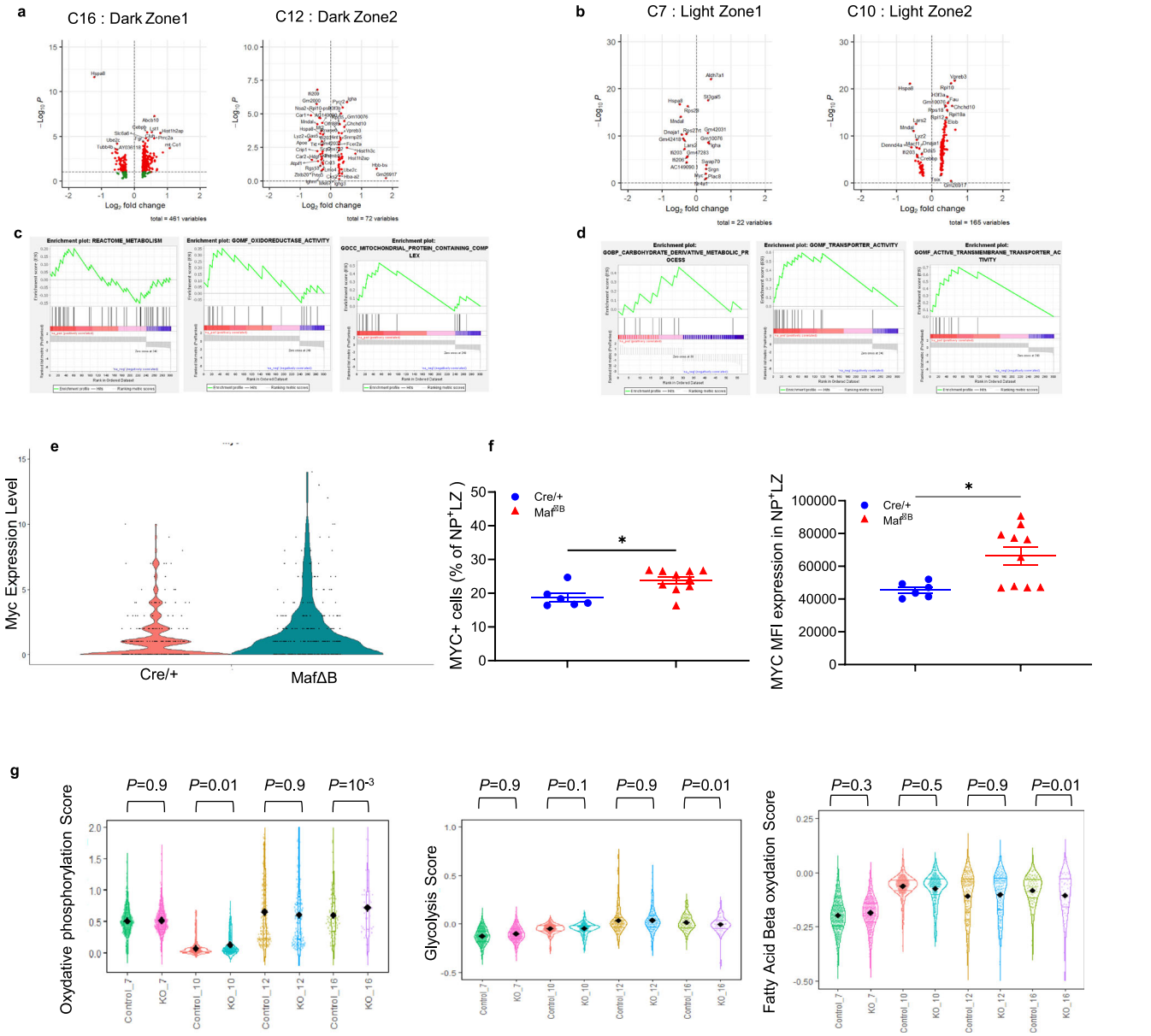

Fig. 8 | Pathway analysis uncovers distinct expression dynamics of OXPHOS metabolism in Maf-deficient GC and PB clusters. a, **b** Volcano plot of upregulated or downregulated genes in $Maf^{\Delta B}$ B cells relative to control B cells in indicated clusters. The red color identifies genes with a fold change >1.2 and a *p*.value < 0.05. **c**, **d** GSEA analysis using ranked genes list of Differential expressed genes (DEG) from the dark zone (DZ; Clusters 16, DZ1 and 12, DZ2) and light zone (LZ; Clusters 7, LZ1 and 10, LZ2). **e** Violin plots of the distribution of *Myc* expression in cluster 7 (LZ1) of $CD19^{Cre/+}$ (Control, red, $N = 2$) and $Maf^{\Delta B}$ (KO, green, $N = 2$) B cells. **f** Percentages (left, $p = 0.02$) and MFI (right, $p = 0.03$) of Myc expressing cells among LZ antigen-specific GC B cells of indicated mice (gated as $NP^{+}CD86^{+}CXCR4^{low}CD38^{low}Fas^{+}$) assessed by flow cytometry. **g** Violin plots of the distribution of OXPHOS, glycolysis and Fatty acid Beta oxidation signature scores in GC clusters (C7: LZ1, C10: LZ2, C12: DZ2 and C16: DZ1) of $CD19^{Cre/+}$ (Control) and $Maf^{\Delta B}$ (KO) B cells. **f** Statistical analysis: unpaired two-tailed Mann–Whitney tests. *$p < 0.05$, ns not significant or ANOVA test using Tukey's correction for multiple comparisons. DEG were calculated using Wilcoxon Rank Sum Test with Benjamini-Hochberg (BH) procedure to adjust p-values. Source data are provided as a Source Data file.

incorporation in vivo, suggesting that Maf does not control cell cycle entry but rather the maintenance and amplification of the cell cycle. Recent studies have underlined that the control of B-cell differentiation into antibody producing cells is linked to cellular proliferation. After initial antigen activation, B cells rapidly proliferate and initiate transcriptional and epigenetic molecular changes[56] resulting in changes in chromatin accessibility in motifs related to essential plasma cell regulators such as IRF4, E2A and c-Rel[57]. The limited impact of Maf deletion on the proliferation of activated B cells between day 3 and day 5 after immunization confirmed that Maf is not involved in the initiation of the proliferation but instead participates in the amplification of PB growth. Along with increased PB numbers, a major consequence of Maf deletion in B cells was the enhancement of cell proliferation within the GC resulting in alteration of the DZ/LZ ratio. This was significant at the early stage of the response (day 5), reaching its maximum by day 7 and persisting until day 12 after the immunization. These results suggest that Maf expression in B cells regulates initial events of the GC reaction and then either becomes dispensable or redundant in more mature GCs. The increased B cell proliferation in the GC directly translated into a boost in post-GC PB generation as shown by the increased number of NP-specific $Bcl6^{low}$ $Irf4^{+}$ cells[33]. Furthermore, our transcriptional analysis has revealed that $Maf^{\Delta B}$ PBs upregulate an

important coactivator of PB differentiation, the positive activator PC4 (encoded by *Sub1*). *Sub1*-deficient B cells exhibit defective plasma cell differentiation upon antigen stimulation, and PC4 reciprocally increases IKAROS and IRF4 protein levels to promote cell survival and plasma cell differentiation[53]. Hence, Maf potentially represses PB differentiation by modulating the PC4/IRF4/IKAROS network.

The control of cell proliferation in the GC represents one of the critical mechanisms governing GC dynamics and output[45]. By restraining B-cell proliferation in the DZ, we hypothesize that Maf reduces the speed of cell cycle transition between DZ and LZ and the recirculation of cells between the two sites. Without Maf, this transition phase increases, accelerating the exit of B cells into PBs with minimal effects on memory B cell generation. Published data support that quiescence versus proliferative status may dictate the outcome of precursor GC into PB *vs* memory B cells as a strict alternative pathway[58,59]. In our study, the increase in PB precursors in the GC of $Maf^{\Delta B}$ mice did not lead to a decrease in the generation of memory B cells, at least at a flow cytometric level, suggesting that these pathways either originate from independent pools of B cells, or develop asynchronously during the GC reaction[60,61]. Although the overall lambda$^+$ (i.e., NP-specific) memory B cell population was similar in immunized $Maf^{\Delta B}$ and WT mice, the slight increase in lambda$^+$IgG$^+$CD80$^-$PDL2$^+$ cells and lambda$^+$IgM$^+$CD80$^-$PDL2$^+$ cells suggests that Maf-deficient B cells may be capable of generating more GCs upon re-immunization[34], though this remains to be tested.

Recent studies have demonstrated that the transcription factor Nr4a1/Nur77 restrains proliferation of activated B cells and that its expression can be used as a surrogate of BCR signaling[62,63]. Our scRNAseq data show that $Maf^{\Delta B}$ LZ cells express significantly higher amounts of *Nr4a1* mRNA, suggesting that deletion of Maf enhances the intensity of the BCR-signaling cascade. Interestingly, IgM-stimulated *Nr4a1* KO B cells display upregulation of Maf expression[64], suggesting a negative feedback regulation exists between the two TFs. Furthermore, similar to what observed in Nr4a1 KO B cells, *Myc* expression is upregulated in Maf KO LZ cells, emphasizing this regulatory circuit. Myc is a master regulator of metabolism, essential for the formation of GCs and their maintenance, and Myc$^+$ cells preferentially localize in the LZ[44,65]. The increase in Myc expression in Maf KO LZ cells correlates with the increase in Myc-targeted genes involved in cell proliferation (*Birc5, Mki67, Ccnb1, Cks2, Hmgn2, Ube2s*, etc.)[66]. Myc expression is directly proportional to the number of cell divisions in the DZ but also to antigen capture and T-cell interaction in the LZ[46]. The observed Myc overexpression in Maf-deficient LZ B cells could either be a consequence of heightened cell proliferation within the GC, or a direct inhibition by Maf. Considering the latter hypothesis, the deletion of Maf would thereby confer an intrinsically competitive advantage over extracellular signals that control Myc expression (strength of the Tfh signal and cytokine signaling). The upregulation of *Icosl* and *Syk* in GC KO cells (in cluster 16) supports this hypothesis.

Our single-cell analysis revealed that Maf regulates numerous metabolic activities during the GC reaction, stressing the link between Maf and Myc in regulating GC biology. Myc regulates glycolysis, oxidative stress and glutaminolysis[67], which are required to ensure the high energetic demand of GC B cells[68,69]. The specialized environment of the GC[70,71] first thought to promote aerobic glycolysis, was recently demonstrated to depend on oxidative phosphorylation (OXPHOS), which engages both mitochondria and peroxisome[50]. This process promotes B-cell clonal expansion, affinity maturation and positive selection[39]. Maf KO GC cells display a specific enrichment in genes involved in oxidative phosphorylation respiratory chain complex, and electron transfer activity (*Nd6, Atp5g3, Atp5d, Cox7a, Cox7b, Cytb*) suggesting that Maf negatively regulate OXPHOS activity to restrain B-cell proliferation and could therefore also modulate BCR affinity. However, although affinity maturation of anti-NP IgG1 was delayed at day 7 in the absence of Maf, it ultimately reached the same level of control B cells, indicating that Maf has no major impact on BCR maturation. Interestingly high ROS (reactive oxygen species) production was linked to increase in Myc activity[51] and required for proliferation in response to BCR stimulation[72]. Recent data have shown that sustained production of ROS leading to mitochondrial dysfunction can increase apoptosis in the GC[73]. Although Maf deletion significantly modifies ROS production, mitochondrial potential appears unaffected, suggesting that this modulation does not lead to a severe mitochondrial defect. This observation is supported by the lack of differences in the proportion of caspase-3-positive cells in the GC. However, there seems to be a feedback mechanism at play, as the initial increase in GC proliferation normalizes after 14 days. This may suggest the existence of compensatory mechanisms from the other member of the MAF transcription factor family such as MafA, MafB, or Mafk, whose association with GC regulation has been demonstrated[74].

IgM and IgG1 antibody responses were significantly higher in $Maf^{\Delta B}$ mice 7 days after T cell-dependent immunization, but these normalized by day 28. We attribute this finding to a decreased number of antigen-specific PCs in $Maf^{\Delta B}$ mice. The fact that Maf-deficient mice exhibit lower numbers of antigen-specific PCs suggests that Maf has a positive regulatory role in the generation and/or maintenance of long-lived plasma cells. This observation agrees with the report that Maf promotes cyclin D2 and integrin beta7 expression in myeloma cells, enhancing their proliferation and survival[75,76]. Thus, it appears that Maf inhibits PBs generation while it promotes plasma cell development. These findings are intriguing because many chronic viral infections associate with short-term PBs and antibody development to the expense of generating long-lived plasma cells that produce more effective and neutralizing antibodies[77,78].

Methods

Mice

All mice were bred and maintained in a specific pathogen-free facility at the University of Colorado AMC Vivarium (Aurora, CO) and used for experiments (both females and males in approximately equal numbers) between 7 and 12 wks of age. All animal procedures were approved by the University of Colorado Denver Institutional Animal Care and Use Committee. The mice were euthanized by cervical dislocation following CO2 exposure. CD19-Cre and loxP-flanked (Maf^{flox}) mice on a C57BL/6J genetic background have been previously described[16,17]. Identification of the Maf^{flox}, Maf^{+}, and Maf^{Δ} alleles was accomplished by PCR on tail genomic DNA using primers MAF forward ATGATCAGGCTCAGGCTTAAA, MAF reverse 1 CGCACCCTGACAACGTG, and MAF reverse 2 CTGGGAAACACAGCAAGCTC that generate PCR fragments 547 bp, 417 bp, and 654 bp, respectively. Mice homozygous for the Maf^{flox} allele and carrying the $CD19^{Cre}$ allele, referred to as $Maf^{\Delta B}$, were generated at the University of Colorado Anschutz Medical Campus (AMC). $Maf^{\Delta B}$ mice were born at the expected mendelian ratio with no obvious abnormalities. CD19-Cre heterozygote mice were used as wild-type controls.

Immunizations

Mice were immunized i.p. with 100 μg $NP_{30\text{-}39}$ (4-Hydroxy-3-nitrophenylacetic) hapten conjugated to CGG (Chicken Gamma Globulin) for T cell-dependent responses, or with 5 μg NP_{32} conjugated to Ficoll (both from Biosearch Technologies) in the presence or not of 100 μg poly(I:C) (polyinosinic-polycytidylic acid; InvivoGen) for TI-2 T cell-independent responses. For TI-1 T cell-independent responses, mice were immunized i.p. with 75 μg of LPS (O111:B4 from E. coli, Invivogen).

RNA extraction and quantitative PCR

B cells were isolated using a Pan B cell isolation kit (Miltenyi Biotec) and an AutoMACS (Miltenyi Biotec) according to the manufacturer's instructions with a purity of >97% based on CD19 and B220 staining. Total RNA was purified using RNAeasy micro-kit (Qiagen) with DNA

removing, and cDNA was synthesized using the SuperScript III First-Strand Synthesis system (Invitrogen). Murine *Maf* cDNAs were amplified using Applied Biosystems TaqMan primer and probe sets (Mm02581355_s1) purchased from Thermo Fisher Scientific. Differences in specific mRNA levels were determined using the deltaCT method normalized to murine 18 s (Mm03928990_g1, AB TaqMan). All samples were run in triplicate using the QuantStudio 7 Flex Real-Time PCR System (Thermo Fisher Scientific).

Cell isolation and cell culture

Organs (bone marrow and spleens) were harvested from euthanized mice. Bone marrow cells were extracted from femurs and shinbones. Single-cell suspensions were incubated for 3 min in ACK lysis buffer (0.15 M NH4Cl, 0.01 M KHCO3, and 0.1 mM EDTA, pH 7.2–7.4) to remove erythrocytes. For cell culture, B cells were enriched by negative selection using the Pan B cell isolation kit (Miltenyi Biotec) and an AutoMACS (Miltenyi Biotec) according to the manufacturer's instructions. B cell purity was consistently >97% based on CD19 and B220 staining. Enriched splenic B cells were cultured at 1×10^6 cells/ml at 37 °C, with 5% CO_2, in complete RPMI-1640 media supplemented with 5% FBS, 1% GlutaMAX, 1% penicillin-streptomycin, 1% nonessential amino acids, and 0.1 M 2-ME for times indicated in the figure legends. For in vitro plasma cell differentiation, splenic B cells were cultured in complete media in the presence of LPS-EB (from E. coli O111:B4, SIGMA) at 10 μg/mL, or anti-CD40 (produced in house, clone 1 C:10) at 1 μg/mL together with recombinant mouse IL-4 (20 ng/mL; Preprotech) and recombinant mouse IL-5 (10 ng/mL; Preprotech) for 4 days. For in vitro cell proliferation assays, splenic B cells were labeled using CellTraceYellow proliferation kit (ThermoFisher) according to manufacturer's instructions. Isolated B cells were incubated in complete RPMI-1640 media in the presence of polyclonal anti-IgM Ab (Jackson Laboratories) at 10 μg/mL, LPS-EB or anti-CD40 with recombinant mouse IL-4 and IL-5 for 4 days.

B-cell phenotyping by spectral flow cytometry

B cell Ab cocktail panels contained combinations of antibodies listed in Supplementary Table 1. NP staining was realized using NP-PE (NIP-CAP-OSu, Biosearch Technologies Cat. N-1110-100 at 1:200 dilution). Prior to staining with Ab cocktails, splenocytes were incubated with the Fc shield anti-mouse CD16/CD32 (clone 2.4G2, Tonbo) Ab and Zombie UV viability dye (1:2000, Biolegend) for 15 min on ice in PBS. All flow cytometry staining was then performed with $2–4 \times 10^6$ splenocytes in PBS containing 1% BSA. For intracellular staining, cells were fixed using Transcription Factor Staining Buffer Set (BD Biosciences) according to the manufacturer's instructions. All flow cytometry data were acquired on the Cytek Aurora and the data were analyzed using FlowJo software (v10.7.1). Splenocytes were used for single color reference controls, except where the use of Ultra Comp eBeads (Invitrogen) was necessary.

In vivo EdU and BrdU assays

Mice were immunized i.p. with 100 μg of NP-CGG in alum. On day 3 post immunization, mice were injected i.p. with 100 μL of 10 mg/mL 5-ethynyl-2′-deoxyuridine (EdU, Invitrogen, Cat. A10044) in PBS and 2 days later, at day 5, with 200 μL of 10 mg/mL 5-bromo-2′-deoxyuridine (BrdU, BD Biosciences, Cat. 559619) in PBS. One hour later, mice were euthanized, spleens harvested, and single-cell suspensions made. Cell staining was performed as described in ref. 28 with slight modifications. Briefly, 2×10^7 splenocytes resuspended in PBS/1% BSA were first incubated with the Fc blocker anti-CD16/32 antibody, followed by staining with PNA-FITC and anti- CD138-BV421, IgG1-PerCP5.5, CD19-BV510, CXCR4-BUV661, B220-BV711, and CD86-BUV563 antibodies (Supplementary Table 1). After washing with PBS/1% BSA, cells were fixed by incubating for 15 min on ice with BD cytofix/cytoperm (BD Biosciences, Cat. 554722). After washing with 2 mL BD Perm/Wash (BD Biosciences, Cat. 554723), cells were incubated in 150 μL permeabilization buffer plus (BD Biosciences, Cat. 561651) on ice for 10 min followed by wash, and 5 min fixation with 150 μL Cytofix/Cytoperm followed by another wash. For DNA digestion, cells were incubated at 37 °C for 1 h in a solution of DNase I at 300 μg/mL in PBS. After washing with Perm/Wash, cells were resuspended in EdU Click-iT reaction mixture (Click-iT Plus EdU Alexa 350 Flow Cytometry Assay Kit, Thermo Fisher) and incubated for 20 min at room temperature. After washing, cells were resuspended in Perm/Wash buffer containing anti-CD16/32 antibody, PE-conjugated NP (Bioresearch), anti-CD95-PE-Cy7 (clone, SA367H8, Biolegend), and anti-BrdU-APC (APC BrdU Flow Kit, BD Biosciences, Cat. 557892) and incubated for 30 min at room temperature. After washing, cells were resuspended in PBS for flow cytometric analysis. Cell staining for EdU in the absence of BrdU staining was performed in accordance to the manufactures protocol (Click-iT Plus EdU Alexa 350 Flow Cytometry Assay Kit, Thermo Fisher) after staining with PNA-FITC and for surface markers with anti- CD138-BV421, CD38-BUV737, IgG1-PerCP5.5, CD19-BV510, CXCR4-BV711, B220-AF700, CD86-APC/Cy7, CD95-PE-Cy7, and lambda-APC (Supplementary Table S1). Before cell acquisition on the flow cytometer, 20 μL of 7AAD solution (BD Biosciences) was added to the samples to analyze for DNA content. Mitochondrial function was assessed using MitoTracker Deep Red (20 nM) and MitoSox (5 μM) from ThermoFisher following the manufacturer's instructions. Briefly, 1×10^6 harvested cells were stained with MitoTracker Deep Red and MitoSox for the evaluation of mitochondrial membrane potential and ROS production, respectively, for 30 min at 37° followed by surface staining for 20 min at 4 °C. Then, cells were washed with PBS and analyzed by flow cytometry.

Measurement of NP-specific antibody by ELISA

To measure NP-specific serum antibody responses, 96-well flat-bottom MaxiSorp MicroWell plates (Thermo Fisher Scientific) were coated overnight with 2 μg/mL NP_{35}–BSA (4-Hydroxy-3-iodo-5-nitrophenylacetyl, Biosearch Technologies) in PBS at 4 °C. Plates were washed once (with PBS, 0.1% Tween 20; Thermo Fisher Scientific), blocked (with PBS, 1% BSA) for 2 h at 37 °C, and washed once again. For capture of antigen-specific antibodies, sera were initially diluted 1:20 or 1:100 and subsequent threefold serial dilutions were made into blocking buffer, and plates were incubated overnight at 4 °C. Plates were washed three times before incubation with an alkaline phosphatase (AP)–conjugated goat anti–mouse isotype-specific detection antibody (SouthernBiotech) for 1 h at 37 °C. After three washes, plates were developed by the addition of alkaline phosphatase substrate buffer consisting of 1 mg/mL 4-nitrophenyl phosphate disodium salt hexahydrate (Alkaline Phosphatase Substrate; Sigma-Aldrich) diluted in 1 M diethanolamine, 8.4 mM MgCl2, and 0.02% NaN3, pH 9.8, and absorbance values read at 405 nm (VersaMax ELISA reader; MDS Analytical Technologies). The following NP-specific mouse mAbs (described in ref. 27) were used as standards to quantify the absolute concentration of NP-specific antibody present in the sera of immunized mice: B1-8μ (NP-specific IgM), S24/63/63 (NP-specific IgG3), N1G9 (NP-specific IgG1), S43-10 (NP-specific IgG2c), and D3-13F1 (NP-specific IgG2b). For affinity maturation measurements, plates were coated with either NP_4–BSA or NP_{35}–BSA capture antigens (Biosearch Technologies) diluted at 2 μg/ml. The ratio of high-affinity antibodies bound to NP_4–BSA relative to the total of both high- and low-affinity antibodies bound to NP_{35}–BSA was calculated as previously described[27].

Serum immunoglobulin isotype-specific ELISAs

Immunoglobulin (Ig) levels in serum were determined by an isotype-specific enzyme-linked immunosorbent assay (ELISA). Briefly, ELISA plates were coated with antibodies against mouse Igs (Southern Biotechnology Associates, Inc). A standard curve was generated by using affinity-purified monoclonal antibodies against mouse IgM, IgG1,

IgG2b, IgG3, and IgG2a/c (Southern Biotechnology Associates, Inc.). The Ig concentration for each individual sample was determined by comparing the mean optical density values from duplicate wells to the standard curve.

Flow cytometric analysis of cell proliferation

Cell proliferation was analyzed by dye dilution using CellTrace Yellow (Thermo Fisher Scientific) according to manufacturer' instructions. Briefly, prior culture, cells were incubated with CellTrace Yellow at 1:500 dilution 20 minutes at 37 °C, then centrifuged in pre-warmed complete culture medium before incubation. After culture, flow cytometry data were acquired on the Cytek Aurora©, and the data were analyzed using the FlowJo'proliferation tool. The "generation 0" peak was set using non-stimulated control cells and represents the undivided cells. The proliferation Index is the total number of divisions divided by the number of cells that went into division taking of account only responding cells. The division Index is the average number of cell divisions in the whole population, including cells which didn't divided during the assay (generation 0).

Single cell RNA sequencing and data processing

Control and $Maf^{\Delta B}$ mice (2 mice per genotype) were immunized i.p. with 100 μg NP-CGG in alum. On day 7, cells from the spleens were harvested and B cells were isolated using the Pan B cell isolation kit (Miltenyi Biotec) and an AutoMACS (Miltenyi Biotec) according to the manufacturer's instructions. B cell purity was >97%. Freshly isolated B cells were loaded into the 10x Genomics instrument and libraries were created using the Single Cell Expression v3.1 (Dual Index) kit (10x Genomics) according to the manufacturer's instructions. FASTQ files were aligned to the mouse *mm10* reference genome using 10x Genomics Cell Ranger software v5.0.1 to create unique molecular identifier count tables of gene expression for each sample. Unique molecular identifier counts were normalized by library size. The UMI count matrix was converted to Seurat objects using R package Seurat (v.4.0.3). Data was cleaned by removing cells with less than 200 genes or more than 10% of UMIs mapped to mitochondrial genes. SCTransform version2 function was used to normalize the dataset[79] and Uniform Manifold Approximation and Projection (UMAP) was used to reduce dimensions. Analysis of GO terms enriched in clusters was done using Enrichr or shinyGO[80], http://bioinformatics.sdstate.edu/go/). Differentiation trajectories were fitted with Slingshot package (version 1.6.1). Differential expressed genes (DEG) were calculated between clusters using the FindMarkers function with a fold change (FC) > 1.2 and a *p*.value < 0.05. Gene set enrichment analysis (GSEA) was performed using ranked gene list of DEG (based on their fold change) between clusters. These lists were processed with the GSEA software from the Broad Institute[81] comparing to the mouse genes set collections (M2, M3, M5 and M8). We applied Topic modeling and Gene signatures score as described in 34031613 using the FitGoM function from the R package CountClust (v.1.12.0), with the number of topics set to 16 and the tolerance value set to 0.5. Genes signatures list used in this study is detailed in Supplementary Data 1. The data have been deposited with links to BioProject accession number PRJNA1002849 in the NCBI BioProject database (https://www.ncbi.nlm.nih.gov/bioproject/?term=PRJNA1002849)

Statistics and data visualization

Data were analyzed using GraphPad Prism software. Statistical significance was determined with the nonparametric Mann–Whitney test or a ANOVA test using Tukey's correction or Fisher's Least Significant Difference (LSD) test for multiple comparisons. The level of significance was established as follows: $*p \le 0.05$; $**p < 0.01$; $***p < 0.001$; $****p < 0.0001$; ns, not significant ($P > 0.05$). Data in graphs are represented as means ± SEM. The mouse used in Figs. 4a, 5a, Supplementary Fig. 3d, e were Created with BioRender.com released under a Creative Commons Attribution-Noncommercial 4.0 International.

Reporting summary

Further information on research design is available in the Nature Portfolio Reporting Summary linked to this article.

Data availability

The data that support the findings of this study are available from the first and the senior authors upon request: sophie.hillion@univ-brest.fr, Roberta.Pelanda@cuanschutz.edu. The data generated in this study are provided in the Supplementary Information/Source Data file provided with this paper. Single cell RNAseq data have been deposited with links to BioProject accession number PRJNA1002849 in the NCBI BioProject database (https://ngdc.cncb.ac.cn/bioproject/browse/insdc/PRJNA1002849). Source data are provided with this paper.

References

1. Blank, V. & Andrews, N. C. The Maf transcription factors: regulators of differentiation. *Trends Biochem. Sci.* **22**, 437–441 (1997).
2. Ring, B. Z. et al. Regulation of mouse lens fiber cell development and differentiation by the Maf gene. *Development* **127**, 307–317 (2000).
3. Kim, J. I. et al. The transcription factor c-Maf controls the production of interleukin-4 but not other Th2 cytokines. *Immunity* **10**, 745–751 (1999).
4. Chihara, N. et al. Induction and transcriptional regulation of the co-inhibitory gene module in T cells. *Nature* **558**, 454–459 (2018).
5. Liu, M. et al. Transcription factor c-Maf is a checkpoint that programs macrophages in lung cancer. *J. Clin. Invest* **130**, 2081–2096 (2020).
6. Parker, M. E. et al. c-Maf regulates the plasticity of group 3 innate lymphoid cells by restraining the type 1 program. *J. Exp. Med.* **217**, e20191030 (2020).
7. Gabrysova, L. et al. c-Maf controls immune responses by regulating disease-specific gene networks and repressing IL-2 in CD4(+) T cells. *Nat. Immunol.* **19**, 497–507 (2018).
8. Andris, F. et al. The Transcription Factor c-Maf Promotes the Differentiation of Follicular Helper T Cells. *Front. Immunol.* **8**, 480 (2017).
9. Vacchio, M. S. et al. A Thpok-Directed Transcriptional Circuitry Promotes Bcl6 and Maf Expression to Orchestrate T Follicular Helper Differentiation. *Immunity* **51**, 465–478 e6 (2019).
10. Ciofani, M. et al. A validated regulatory network for Th17 cell specification. *Cell* **151**, 289–303 (2012).
11. Zhang, H. et al. An IL-27-Driven Transcriptional Network Identifies Regulators of IL-10 Expression across T Helper Cell Subsets. *Cell Rep.* **33**, 108433 (2020).
12. Morito, N. et al. A novel transgenic mouse model of the human multiple myeloma chromosomal translocation t(14;16)(q32;q23). *Cancer Res.* **71**, 339–348 (2011).
13. Jiang, Q. et al. Targeting the oncogenic transcription factor c-Maf for the treatment of multiple myeloma. *Cancer Lett.* **543**, 215791 (2022).
14. Michee-Cospolite, M. et al. Molecular Mechanisms Driving IL-10-Producing B Cells Functions: STAT3 and c-MAF as Underestimated Central Key Regulators? *Front Immunol.* **13**, 818814 (2022).
15. Radomir, L. et al. The survival and function of IL-10-producing regulatory B cells are negatively controlled by SLAMF5. *Nat. Commun.* **12**, 1893 (2021).
16. Wende, H. et al. The transcription factor c-Maf controls touch receptor development and function. *Science* **335**, 1373–1376 (2012).

17. Rickert, R. C., Roes, J. & Rajewsky, K. B lymphocyte-specific, Cre-mediated mutagenesis in mice. *Nucleic Acids Res.* **25**, 1317–1318 (1997).
18. Soon, M. S. F. et al. Transcriptome dynamics of CD4(+) T cells during malaria maps gradual transit from effector to memory. *Nat. Immunol.* **21**, 1597–1610 (2020).
19. Hardy, R. R. & Hayakawa, K. B cell development pathways. *Annu. Rev. Immunol.* **19**, 595–621 (2001).
20. Minnich, M. et al. Multifunctional role of the transcription factor Blimp-1 in coordinating plasma cell differentiation. *Nat. Immunol.* **17**, 331–343 (2016).
21. Tellier, J. et al. Blimp-1 controls plasma cell function through the regulation of immunoglobulin secretion and the unfolded protein response. *Nat. Immunol.* **17**, 323–330 (2016).
22. Smith, F. I., Tesch, H. & Rajewsky, K. Heterogeneous and monoclonal helper T cells induce similar anti-(4-hydroxy-3-nitrophenyl) acetyl (NP) antibody populations in the primary adoptive response. II. Lambda light chain dominance and idiotope expression. *Eur. J. Immunol.* **14**, 195–200 (1984).
23. Han, S. et al. In situ studies of the primary immune response to (4-hydroxy-3-nitrophenyl)acetyl. IV. Affinity-dependent, antigen-driven B cell apoptosis in germinal centers as a mechanism for maintaining self-tolerance. *J. Exp. Med.* **182**, 1635–1644 (1995).
24. Li, Y. et al. EAF2 mediates germinal centre B-cell apoptosis to suppress excessive immune responses and prevent autoimmunity. *Nat. Commun.* **7**, 10836 (2016).
25. Weisel, F. J. et al. A Temporal Switch in the Germinal Center Determines Differential Output of Memory B and Plasma Cells. *Immunity* **44**, 116–130 (2016).
26. Roco, J. A. et al. Class-Switch Recombination Occurs Infrequently in Germinal Centers. *Immunity* **51**, 337–350 e7 (2019).
27. Swanson, C. L. et al. Type I IFN enhances follicular B cell contribution to the T cell-independent antibody response. *J. Exp. Med.* **207**, 1485–1500 (2010).
28. Zotos, D. et al. The concerted change in the distribution of cell cycle phases and zone composition in germinal centers is regulated by IL-21. *Nat. Commun.* **12**, 7160 (2021).
29. Chen, C. et al. Uhrf1 regulates germinal center B cell expansion and affinity maturation to control viral infection. *J. Exp. Med.* **215**, 1437–1448 (2018).
30. Gitlin, A. D. et al. HUMORAL IMMUNITY. T cell help controls the speed of the cell cycle in germinal center B cells. *Science* **349**, 643–646 (2015).
31. Maltsev, D. I. et al. The bioavailability time of commonly used thymidine analogues after intraperitoneal delivery in mice: labeling kinetics in vivo and clearance from blood serum. *Histochem Cell Biol.* **157**, 239–250 (2022).
32. Pae, J. et al. Cyclin D3 drives inertial cell cycling in dark zone germinal center B cells. *J. Exp. Med.* **218**, e20201699 (2021).
33. Ise, W. et al. T Follicular Helper Cell-Germinal Center B Cell Interaction Strength Regulates Entry into Plasma Cell or Recycling Germinal Center Cell Fate. *Immunity* **48**, 702–715.e4 (2018).
34. Zuccarino-Catania, G. V. et al. CD80 and PD-L2 define functionally distinct memory B cell subsets that are independent of antibody isotype. *Nat. Immunol.* **15**, 631–637 (2014).
35. Lalor, P. A. et al. Functional and molecular characterization of single, (4-hydroxy-3-nitrophenyl)acetyl (NP)-specific, IgG1+ B cells from antibody-secreting and memory B cell pathways in the C57BL/6 immune response to NP. *Eur. J. Immunol.* **22**, 3001–3011 (1992).
36. Qin, X. F. et al. OCA-B integrates B cell antigen receptor-, CD40L- and IL 4-mediated signals for the germinal center pathway of B cell development. *EMBO J.* **17**, 5066–5075 (1998).
37. Blanc, P. et al. Mature IgM-expressing plasma cells sense antigen and develop competence for cytokine production upon antigenic challenge. *Nat. Commun.* **7**, 13600 (2016).
38. Pracht, K. et al. A new staining protocol for detection of murine antibody-secreting plasma cell subsets by flow cytometry. *Eur. J. Immunol.* **47**, 1389–1392 (2017).
39. Chen, D. et al. Coupled analysis of transcriptome and BCR mutations reveals role of OXPHOS in affinity maturation. *Nat. Immunol.* **22**, 904–913 (2021).
40. Grenov, A. et al. YTHDF2 suppresses the plasmablast genetic program and promotes germinal center formation. *Cell Rep.* **39**, 110778 (2022).
41. Mathew, N. R. et al. Single-cell BCR and transcriptome analysis after influenza infection reveals spatiotemporal dynamics of antigen-specific B cells. *Cell Rep.* **35**, 109286 (2021).
42. Victora, G. D. et al. Germinal center dynamics revealed by multiphoton microscopy with a photoactivatable fluorescent reporter. *Cell* **143**, 592–605 (2010).
43. La Manno, G. et al. RNA velocity of single cells. *Nature* **560**, 494–498 (2018).
44. Calado, D. P. et al. The cell-cycle regulator c-Myc is essential for the formation and maintenance of germinal centers. *Nat. Immunol.* **13**, 1092–1100 (2012).
45. De Silva, N. S. & Klein, U. Dynamics of B cells in germinal centres. *Nat. Rev. Immunol.* **15**, 137–148 (2015).
46. Finkin, S. et al. Protein Amounts of the MYC Transcription Factor Determine Germinal Center B Cell Division Capacity. *Immunity* **51**, 324–336 e5 (2019).
47. Wilker, P. R. et al. Transcription factor Mef2c is required for B cell proliferation and survival after antigen receptor stimulation. *Nat. Immunol.* **9**, 603–612 (2008).
48. Wohner, M. et al. Molecular functions of the transcription factors E2A and E2-2 in controlling germinal center B cell and plasma cell development. *J. Exp. Med.* **213**, 1201–1221 (2016).
49. Boothby, M. & Rickert, R. C. Metabolic Regulation of the Immune Humoral Response. *Immunity* **46**, 743–755 (2017).
50. Weisel, F. J. et al. Germinal center B cells selectively oxidize fatty acids for energy while conducting minimal glycolysis. *Nat. Immunol.* **21**, 331–342 (2020).
51. Jang, K. J. et al. Mitochondrial function provides instructive signals for activation-induced B-cell fates. *Nat. Commun.* **6**, 6750 (2015).
52. Gloury, R. et al. Dynamic changes in Id3 and E-protein activity orchestrate germinal center and plasma cell development. *J. Exp. Med.* **213**, 1095–1111 (2016).
53. Ochiai, K. et al. Chromatin Protein PC4 Orchestrates B Cell Differentiation by Collaborating with IKAROS and IRF4. *Cell Rep.* **33**, 108517 (2020).
54. Shaffer, A. L. et al. IRF4 addiction in multiple myeloma. *Nature* **454**, 226–231 (2008).
55. Oliver, A. M., Martin, F. & Kearney, J. F. IgMhighCD21high lymphocytes enriched in the splenic marginal zone generate effector cells more rapidly than the bulk of follicular B cells. *J. Immunol.* **162**, 7198–7207 (1999).
56. Scharer, C. D. et al. Plasma cell differentiation is controlled by multiple cell division-coupled epigenetic programs. *Nat. Commun.* **9**, 1698 (2018).
57. Roy, K. et al. A Regulatory Circuit Controlling the Dynamics of NFkappaB cRel Transitions B Cells from Proliferation to Plasma Cell Differentiation. *Immunity* **50**, 616–628 e6 (2019).
58. Cancro, M. P. & Tomayko, M. M. Memory B cells and plasma cells: The differentiative continuum of humoral immunity. *Immunol. Rev.* **303**, 72–82 (2021).
59. Inoue, T. et al. Exit from germinal center to become quiescent memory B cells depends on metabolic reprograming and provision of a survival signal. *J. Exp. Med.* **218**, e20200866 (2021).
60. Suan, D., Sundling, C. & Brink, R. Plasma cell and memory B cell differentiation from the germinal center. *Curr. Opin. Immunol.* **45**, 97–102 (2017).

61. Shinnakasu, R. et al. Regulated selection of germinal-center cells into the memory B cell compartment. *Nat. Immunol.* **17**, 861–869 (2016).
62. Brooks, J. F. et al. Negative feedback by NUR77/Nr4a1 restrains B cell clonal dominance during early T-dependent immune responses. *Cell Rep.* **36**, 109645 (2021).
63. Glaros, V. et al. Limited access to antigen drives generation of early B cell memory while restraining the plasmablast response. *Immunity* **54**, 2005–2023.e10 (2021).
64. Tan, C. et al. NR4A nuclear receptors restrain B cell responses to antigen when second signals are absent or limiting. *Nat. Immunol.* **21**, 1267–1279 (2020).
65. Dominguez-Sola, D. et al. The proto-oncogene MYC is required for selection in the germinal center and cyclic reentry. *Nat. Immunol.* **13**, 1083–1091 (2012).
66. Yu, D. et al. Functional validation of genes implicated in lymphomagenesis: an in vivo selection assay using a Myc-induced B-cell tumor. *Ann. N.Y. Acad. Sci.* **1059**, 145–159 (2005).
67. Goetzman, E. S. & Prochownik, E. V. The Role for Myc in Coordinating Glycolysis, Oxidative Phosphorylation, Glutaminolysis, and Fatty Acid Metabolism in Normal and Neoplastic Tissues. *Front. Endocrinol.* **9**, 129 (2018).
68. Choi, S. C. & Morel, L. Immune metabolism regulation of the germinal center response. *Exp. Mol. Med.* **52**, 348–355 (2020).
69. Ersching, J. et al. Germinal Center Selection and Affinity Maturation Require Dynamic Regulation of mTORC1 Kinase. *Immunity* **46**, 1045–1058.e6 (2017).
70. Cho, S. H. et al. Germinal centre hypoxia and regulation of antibody qualities by a hypoxia response system. *Nature* **537**, 234–238 (2016).
71. Jellusova, J. et al. Gsk3 is a metabolic checkpoint regulator in B cells. *Nat. Immunol.* **18**, 303–312 (2017).
72. Wheeler, M. L. & Defranco, A. L. Prolonged production of reactive oxygen species in response to B cell receptor stimulation promotes B cell activation and proliferation. *J. Immunol.* **189**, 4405–4416 (2012).
73. Inoue, T. et al. Csk restrains BCR-mediated ROS production and contributes to germinal center selection and affinity maturation. *J. Exp. Med.* **221**, e20231996 (2024).
74. Huang, C. et al. Cooperative transcriptional repression by BCL6 and BACH2 in germinal center B-cell differentiation. *Blood* **123**, 1012–1020 (2014).
75. Kienast, J. & Berdel, W. E. c-maf in multiple myeloma: an oncogene enhancing tumor-stroma interactions. *Cancer Cell* **5**, 109–110 (2004).
76. Rasmussen, T. et al. C-MAF oncogene dysregulation in multiple myeloma: frequency and biological relevance. *Leuk. Lymphoma* **44**, 1761–1766 (2003).
77. Cooper, L. & Good-Jacobson, K. L. Dysregulation of humoral immunity in chronic infection. *Immunol. Cell Biol.* **98**, 456–466 (2020).
78. Schweier, O. et al. Residual LCMV antigen in transiently CD4(+) T cell-depleted mice induces high levels of virus-specific antibodies but only limited B-cell memory. *Eur. J. Immunol.* **49**, 626–637 >(2019).
79. Choudhary, S. & Satija, R. Comparison and evaluation of statistical error models for scRNA-seq. *Genome Biol.* **23**, 27 (2022).
80. Ge, S. X., Jung, D. & Yao, R. ShinyGO: a graphical gene-set enrichment tool for animals and plants. *Bioinformatics* **36**, 2628–2629 (2020).
81. Subramanian, A. et al. Gene set enrichment analysis: a knowledge-based approach for interpreting genome-wide expression profiles. *Proc. Natl Acad. Sci. USA* **102**, 15545–15550 (2005).

Acknowledgements

We are grateful to Carmen Birchmeier and Michael Strehle (Max-Delbruck Centrum for Molecular Medicine) for the gift of Maf-floxed mice. We acknowledge the ImmunoMicro Flow Cytometry Shared Resource Laboratory (RRID:SCR_021321), the Vivarium, and the Genomics and Microarray Shared Resource (RRID:SCR_021984) at the University of Colorado Anschutz Medical Campus. We also acknowledge the members of the Pelanda lab and Torres lab for helpful discussions. We appreciate the help of Moriah Castleman in editing the manuscript. We acknowledge the Cytometry Core Facility Hyperion (Brest, France) for access to their instruments. We thank Julie Hocquelet and Stéphanie Deshayes from the LBAI for their technical assistance. This work was supported by the National Institute of Health grants R21 AI156232 (to R.P. and S.H.) and AI136534 (to R.M.T.). R.P. salary was also partly supported by grant AI152535, and R.T. salary was partly supported by grant AI143261. This work was also partly supported by the Cancer Center Support Grant P30CA046934 and by the Labex IGO program (n° ANR-11-LBX-0016) funded by the "Investment into the Future" French Government program, managed by the National Research Agency.

Author contributions

S.H. and R.P. designed the study, interpreted the work, and wrote the manuscript. S.H. and A.M. performed experiments and analyzed the data. L.L.P. provided help for ELISA experiments. C.L.D. provided help for single-cell RNA sequencing analysis. M.B. and D.C. helped interpret results. R.M. Torres provided some reagents and methods and edited the manuscript. All authors reviewed and edited the manuscript.

Competing interests

The authors declare no competing interests.

Additional information

Supplementary information The online version contains supplementary material available at https://doi.org/10.1038/s41467-024-52224-6.

Correspondence and requests for materials should be addressed to Sophie Hillion.

Peer review information *Nature Communications* thanks the anonymous reviewer(s) for their contribution to the peer review of this work. A peer review file is available.